Article:
Sarrami-Foroushani, A, Lassila, T orcid.org/0000-0001-8947-1447 and Frangi, AF orcid.org/0000-0002-2675-528X (2017) Virtual endovascular treatment of intracranial aneurysms: models and uncertainty. WIREs: Systems Biology and Medicine, 9 (4). e1385. ISSN 1939-5094

https://doi.org/10.1002/wsbm.1385

WIREs
SYSTEMS BIOLOGY AND MEDICINE

WILEY

Virtual endovascular treatment of intracranial aneurysms: models and uncertainty

Journal:	*WIREs Systems Biology and Medicine*
Manuscript ID	SYSBIO-348.R1
Wiley - Manuscript type:	Advanced Review
Date Submitted by the Author:	09-Jan-2017
Complete List of Authors:	Sarrami-Foroushani, Ali; University of Sheffield Lassila, Toni; University of Sheffield Frangi, Alejandro; University of Sheffield,
Choose 1-3 topics to categorize your article:	Computational Methods (2COM) < Analytical and Computational Methods (ACM)

WIREs Wiley Interdisciplinary Reviews

Article Title: **Virtual endovascular treatment of intracranial aneurysms: models and uncertainty**

Article Type:

☐ OPINION ☐ PRIMER ☐ OVERVIEW

☒ ADVANCED REVIEW ☐ FOCUS ARTICLE ☐ SOFTWARE FOCUS

Authors:

Full name and affiliation; email address if corresponding author; any conflicts of interest

First author Ali Sarrami-Foroushani Center for Computational Imaging and Simulation Technologies in Biomedicine (CISTIB), The University of Sheffield, UK.
Second author Toni Lassila Center for Computational Imaging and Simulation Technologies in Biomedicine (CISTIB), The University of Sheffield, UK.
Third author Alejandro F. Frangi* Center for Computational Imaging and Simulation Technologies in Biomedicine (CISTIB), The University of Sheffield, UK. a.frangi@sheffield.ac.uk

Authors have no conflicts of interests to declare.

Abstract

Virtual endovascular treatment models (VETMs) have been developed with the view to aid interventional neuroradiologists and neurosurgeons to pre-operatively analyse the comparative efficacy and safety of endovascular treatments for intracranial aneurysms. Based on the current state of VETMs in aneurysm rupture risk stratification and in patient-specific prediction of treatment outcomes, we argue there is a need to go beyond personalised biomechanical flow modelling assuming deterministic parameters and error-free measurements. The mechanobiological effects associated with blood clot formation are important factors in therapeutic decision making and models of post-treatment intra-aneurysmal biology and biochemistry should be linked to the current purely haemodynamic models to improve the predictive power of current VETMs. The influence of model and parameter uncertainties associated to each component of a VETM are, where feasible, quantified via a random-effects meta-analysis of the literature. This allows estimating the pooled effect size of these uncertainties on aneurysmal wall shear stress. From such meta-analyses, two main sources of uncertainty emerge where research efforts have so far been limited: i) vascular wall distensibility, and ii) intra/inter-subject systemic flow variations. In the future, we suggest that current deterministic computational simulations need to be extended with strategies for uncertainty mitigation, uncertainty exploration, and sensitivity reduction techniques.

Graphical/Visual Abstract and Caption

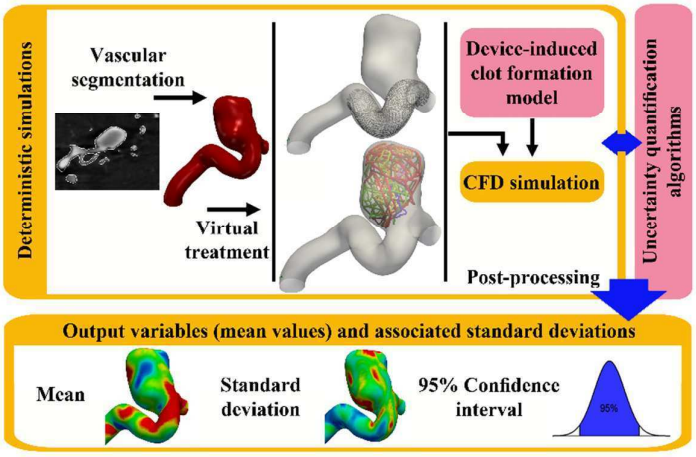

An ideal virtual endovascular treatment model is comprised of sub-models in which the vascular surface, virtual treatment, and mechanobiology of clot formation are modelled, respectively. Uncertainty quantification techniques should be added to the deterministic models to propagate uncertainties through the models and produce confidence intervals associated with the model predictions.

Introduction

Intracranial aneurysms (IAs) are pathological dilatations of the intracranial arteries that commonly occur in various locations around the circle of Willis in approximately 5-8% of the general population [1]. Aneurysm rupture causes subarachnoid haemorrhage, which is associated with high rates of morbidity, mortality, and long term disability [1]. The clinical strategy for treating aneurysms is to isolate them from the circulation, which is commonly performed either by open surgery (clipping the aneurysm), or by endovascular treatment (catheter insertion of a flow diverter or a coil within the aneurysm). In each method, isolation is aimed at creating conditions of blood stasis leading to the generation of a stable clot in the aneurysm sac (embolisation). Once the aneurysm has occluded completely, a neo-intimal layer forms over the aneurysm neck and separates the aneurysm from the circulatory system (endothelialisation). Although it might be addressed as more advanced interventional techniques become available, currently, aneurysms treated with endovascular techniques are more likely to recur than those treated surgically [2]. However, the non-invasiveness of the endovascular approaches has made them more favourable options for treatment of IAs.

Recent progress made in diagnostic techniques over the past few decades has increased the detection rate of unruptured IAs [3]. This has consequently posed the dilemma of whether every unruptured aneurysm must be treated immediately upon discovery, and if so, which treatment option represents the least risk to the patient [2, 4, 5]. The challenge is therefore to evaluate the safety and efficacy of different endovascular treatments in a patient-specific context. Post-treatment ruptures, aneurysm recurrence or incomplete occlusion, and thromboembolic complications after endovascular treatment further magnify the importance of choosing an appropriate endovascular treatment option. Clinicians' attempts at answering such questions has revealed the need for tools that help them in reliable risk assessment and designing appropriate patient-specific treatment plans for each individual aneurysm.

The important role of haemodynamics in the initiation, progression, and rupture of aneurysms has drawn the research community's attention to image-based computational fluid dynamics simulations. Such tools would allow researchers to study the haemodynamic variables in each specific aneurysm pre- and post-operation. Exploiting recent advancements in image segmentation and computational mechanics, virtual endovascular treatment models (VETMs) have been developed to create image-based patient-specific models of aneurysm geometries [6-8], to virtually deploy endovascular devices [9-12], and to simulate intra-aneurysmal blood flow [13-15]. This has allowed investigating how safely and effectively each device deployment strategy alters the intra-aneurysmal haemodynamics, and to which extent the altered intra-aneurysmal flow is favourable to the formation of a stable clot, leading finally to complete aneurysm occlusion and elimination [15, 16]. Moreover, such endovascular treatment models help clinicians to pre-operatively and assess the candidate treatment options and deployment strategies; especially in complex cases like anatomically complex and surgically inaccessible vertebrobasilar dolichoectasia with fusiform aneurysms [17, 18], or aneurysms at/near bifurcations where the neighbouring branches/perforators are in the risk of being covered and occluded [19].

The identification of an appropriate metric to assess post-operative performance of the endovascular treatment is still an active area of research. Different flow and wall shear stress-related quantities have been proposed for this purpose. Localised low and oscillatory aneurysmal wall shear stress (WSS) can lead to pathological endothelial responses, thrombosis, wall degeneration, and eventual aneurysm rupture [20]. On the other hand, endovascular devices are shown to trigger the aneurysm healing process by inducing flow stasis and thrombosis inside the aneurysm sac [2]. However, it is not clear why low shear-induced thrombosis may lead to complete embolisation in some aneurysms, but incomplete embolisation and rupture in some others [21, 22]. Kulcsar et al. [21]

hypothesised that the quality, quantity, and evolution of the thrombus and consequently the thrombus-induced autolytic activities in the wall, determine whether intra-aneurysmal thrombus generation leads to aneurysm healing or rupture. This implies that the endovascular device performance should be assessed in terms of the capability to induce a stable clot, which triggers the process of reverse remodelling and aneurysm healing, possibly accounting for the effect of coadjuvant blood-thinning pharmacological agents. Therefore, although post-operative aneurysmal haemodynamics play an important role in the outcome of the intervention, a VETM should incorporate information about device-induced biochemistry and mechanobiology for assessing its performance for making predictions about aneurysm occlusion and treatment outcomes. Such information can be provided either by phenomenological sub-models that use haemodynamics as a surrogate of intra-aneurysmal biochemistry and biology [23-25], or by more complex mechanistic sub-models, which are coupled to the haemodynamic sub-models and describe the ongoing biological process[23, 26, 27]. Consequently, as shown in Figure 1, an ideal VETM is comprised of: 1) a computational blood flow simulation in an image-based vascular surface model coupled with proper boundary conditions, 2) an endovascular device deployment model, and 3) a blood coagulation model, which describes the intra-aneurysmal clot formation process in the presence of endovascular devices.

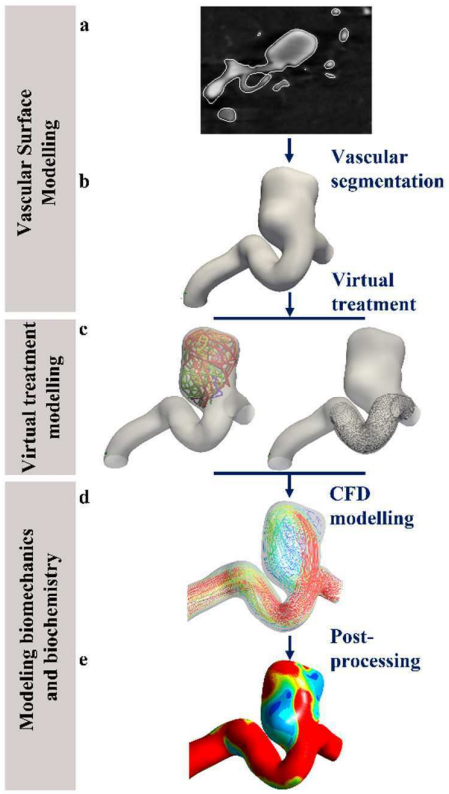

Figure 1. An ideal virtual endovascular treatment model is comprised of sub-models in which the vascular surface, virtual treatment, and biomechanics and biochemistry are modelled, respectively. Patient's angiogram (a) is segmented and a vascular surface model (b) is reconstructed and used for virtual treatment with coils or flow diverting stents (c). CFD simulations then are performed to calculate blood velocity field (d) in the presence of device-induced intra-aneurysmal clot, from which the shear stresses on the vessel wall (e) can be computed.

In 2012, Kallmes [28] raised concerns about the clinical relevance of computational models by arguing that they are prone to several sources of *uncertainty and error* that influence the model predictions. Despite many advancements bridging some of the gaps between model predictions and actual physiological phenomena, the characterisation of the uncertainties and errors associated with the model inputs, and the sensitivity of personalised haemodynamic predictions require more detailed investigation. Uncertainties arise from lack of personalised information about some model inputs, imprecise model structures, e.g. mathematical descriptions of the biological phenomena, and inherent inter- and intra-subject variabilities of physiological variables. As depicted in Figure 2, uncertainty quantification can be performed to identify and quantify uncertainties in the model inputs. Similarly, error analyses can be performed to identify and quantify errors in the deterministic inputs that are not uncertain but can produce errors if not selected properly, e.g. computational meshes. In order to reliably represent the patient-specific physiological processes and achieve truly clinically relevant predictions, it is important that these uncertainties and errors be propagated into the model predictions through sensitivity analyses, and be eliminated when possible.

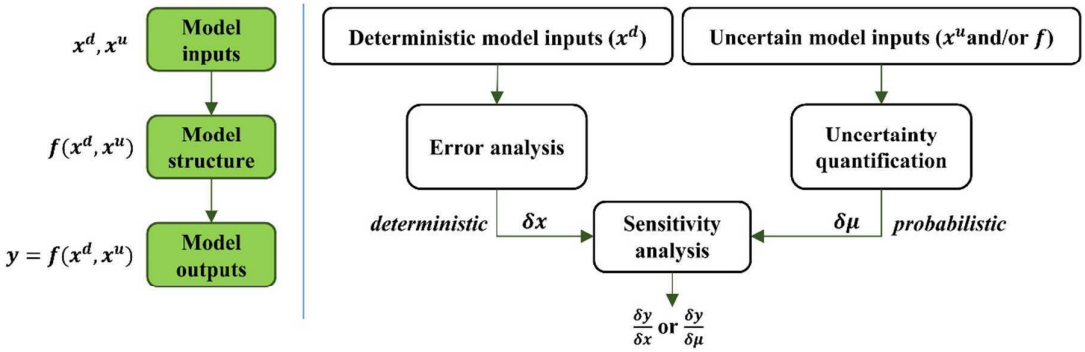

Figure 2. The left panel shows overall structure of a typical mathematical model with x^d and x^u as vectors of deterministic and uncertain model inputs, respectively; f describing the model structure; and y as vector of model outputs. The right panel shows error analysis and uncertainty quantification as processes to identify and quantify errors and uncertainties, respectively; and sensitivity analysis as a process to propagate the quantified errors and uncertainties to the model outputs.

We address the state of different sub-models of a typical VETM based on a comprehensive literature review of the articles focused on computational models of intracranial aneurysms and published online before June 2016. For each sub-model, we discuss the possible sources of uncertainty and error, and, where they exist, review the sensitivity analyses that have been done to show how model predictions are affected by either the uncertain inputs or errors in the deterministic inputs. For simplicity, from now on, we denote both uncertain inputs and errors in deterministic inputs as *uncertainty* throughout the paper. In order to summarise the effect of uncertain inputs, meta-analyses are conducted where the following criteria are met: 1) the study was numerical, performed on the intracranial aneurysms, and published between January 2006 to June 2016, 2) at least 3 cases were studied, and 3) the effect of uncertain model inputs on the aneurysmal WSS was investigated and quantitative values of WSS were reported. For those sources of uncertainties where a sufficient number of studies provided evidence, effect sizes are calculated as standardised mean differences (Hedges' *g*) between the two non-independent groups in each study and then are pooled across studies using random-effects meta-analysis [29]. Finally, we summarise the most important uncertainties that should be addressed in order to present patient-specific predictions to enable such simulations to be reliably used in clinical practice.

Vascular surface and blood flow modelling

Image-based patient-specific vascular surface modelling

Creating vascular surface models from medical images is the first and most important step in developing a patient-specific model for endovascular treatment of aneurysms [13], on which all the other steps depend. Vascular angiograms are usually acquired using computed tomography angiography (CTA) [30], magnetic resonance angiography (MRA) [31], or three-dimensional rotational angiography (3DRA) [32]. The spatial resolution of 3DRA (128^2-512^2 matrix with voxel size of 0.42-1 mm) is usually higher than CTA (512^2 matrix with pixel size of 0.23-0.45 mm and slice thickness of 0.5-1.3 mm) and MRA (256^2 matrix with pixel size of 0.78-1.25 mm and slice thickness of 0.7-1.6 mm) [6]. Piontin et al. [33] assessed the accuracy of 3DRA, CTA, and MRA techniques for measuring the volume of an in vitro model of an anterior communicating artery aneurysm. They showed that CTA is more accurate than MRA (*p*-value = 0.0019), and 3DRA is more accurate than CTA, (*p*-value = 0.1605; not statistically significant). They observed that aneurysm volume was overestimated by 7% and 11.3% in 3DRA and CTA, respectively, and underestimated by 15% in MRA images. Ramachandran et al. [34] reported that errors in measuring aneurysm characteristic lengths (e.g., height and maximum diameter) by any of the 3DRA, CTA, and MRA were 0.8-4%, with no significant differences between the modalities. In clinical practice, due to the less invasive nature of CTA and MRA, these imaging techniques are favoured for the diagnosis and monitoring of intracranial aneurysms; however, 3DRA provides the highest spatial resolution and is consequently favoured for surgical or endovascular treatment planning [35-37]. On the other hand, high spatial and contrast resolution and no interference of bony structures and surrounding tissues in 3DRA images, and consequently their ease of reconstruction, make them more appropriate for construction of 3D aneurysm surface models that can subsequently be used in CFD analyses and virtual treatment models [6, 33, 38, 39].

Starting from volumetric medical images, different techniques have been proposed for segmentation and creation of vascular surface models, which can then be used for generating a computational volumetric mesh and solving blood flow equations. In this paper, we only review methods which have been tested and evaluated on intracranial aneurysms. The need for contrast injection into the feeding artery of the aneurysm exposes the 3DRA modality to limitations when aneurysms with multiple feeding arteries are being scanned. Castro et al. [38] proposed a segmentation methodology, which combined image co-registration and surface merging techniques to overcome this limitation, and provided surface models for aneurysms with multiple inlet branches such as those located on the anterior communicating arteries. They evaluated their method on a virtual 3D rotational angiogram of a digital phantom of an anterior communicating artery aneurysm. The maximum distance between the segmented and phantom model (0.2 mm) was reported as a measure of accuracy. Chang et al. [6] proposed another segmentation methodology called charged fluid-based aneurysm segmentation (CFAS), which combined a region-growing method with the 3D extension of a deformable contour based on a charged fluid model. Their method was particularly designed for segmentation of aneurysms with different geometrical complexity levels and was evaluated on 3DRA images of 15 aneurysms. Comparing segmented surfaces with the manually delineated contours, a conformity score of 68.36% was reported. A knowledge-based segmentation algorithm based on the geodesic active regions (GAR) was presented by Hernandez and Frangi [8] and evaluated by segmentation of intracranial aneurysms from CTA (10 aneurysms) and 3DRA (5 aneurysms) images. They reported average Dice Similarity Coefficients (DSC) of 91.13% and 73.31% as measures of accuracy for 3DRA and CTA images, respectively. Bogunovic et al. [40] proposed another methodology for segmenting 3DRA images based on an image intensity standardisation (IIS) –method, which improved the automation of knowledge-based vascular segmentation algorithms by standardisation of image intensity ranges of tissue classes in routine medical images. They evaluated the method on 10 patients that underwent both 3DRA and TOF-MRA. DSC scores of 92% and 91% was achieved for segmentations from 3DRA and MRA images, respectively. Firouzian et al. [7] proposed another

segmentation technique for segmenting aneurysms from CTA modality, which worked based on geodesic active contours (GAC) and did not require image intensity training unlike when working with knowledge-based methods. They evaluated the method on 11 aneurysms and reported a DSC score of 82.1% as a measure of accuracy. A detailed review of the above mentioned methods can be found in [13-15, 41] with more details. Comparisons of different segmentation techniques for intracranial aneurysms can also be found in [40, 42].

Uncertainty in vascular surface modelling

Uncertainties in the vascular geometric models can originate from images used to reconstruct the vascular surfaces. Such uncertainties include the inherent noise in the acquired images, registration artefacts, and motion of arteries during the cardiac cycle. Depending on the operator's experience and skill, manual operations during image acquisition may also lead to errors in the acquired images. Another more important source of uncertainty in vascular surface modelling are segmentation errors. Despite automation of the segmentation process in most state-of-the-art segmentation methods, manual editing operations are still required in the final stages, especially where complex structures like small or kissing branches are present in the region of interest.

Cebral et al. [13] performed a sensitivity analysis on different uncertain aspects of an image-based model. They qualitatively showed that the geometric uncertainties arising from segmentation of aneurysm surfaces by different operators has the greatest effect on the intra-aneurysmal flow when compared to uncertainties in other variables. Castro et al. [43] investigated the effect of parent vessel reconstruction on the flow in the aneurysm sac. For each aneurysm they constructed two different models; one with the original parent vessel and the other with a truncated parent vessel, which was replaced with a straight tube. They observed an underestimation of aneurysmal WSS in geometric models with a truncated parent vessel and showed that segmentation of the parent vessel can highly affect the characteristic flow patterns inside aneurysm. As a future work, they suggested a sensitivity analysis for typical aneurysms of different locations, which gives an estimation of the length of the upstream parent vessel needed for an appropriate simulation of flow inside the aneurysm. Gambaruto et al. [44] compared the effect of the smoothing level, as part of the segmentation procedure, with the effect of the blood rheological model on the intra-aneurysmal flow and aneurysmal WSS. They showed that geometric uncertainties due to the use of different smoothing levels resulted in greater errors (of order of 15%), although this was comparable with errors arising from using different blood rheological models (of order of 5%). Geers et al. [39, 45], performed CFD simulations in aneurysm models reconstructed from CTA and 3DRA images. They showed that the main flow characteristics remains the same in aneurysms obtained from both modalities but a difference of up to 44.2% was observed in the absolute value of mean WSS on the aneurysm sac.

Blood flow modelling

In order to simulate blood flow in the reconstructed vascular volume, equations of motion for blood flow need to be discretised and solved. This requires a volumetric mesh over the domain confined by the vascular surface mesh. Vascular surface meshes are usually extruded at the truncated boundaries to minimise the effects of boundary conditions on the domain of interest (i.e., the aneurysm) Tetrahedral or polyhedral elements are commonly used to discretise the volume [46]. To accurately address high velocity radial gradients in vicinity of the wall, and thus to accurately estimate the WSS, three to five layers of prismatic boundary layer elements are required in near-wall regions [13, 47, 48]. Unstructured meshes in the context of aneurysm flow modelling are commonly comprised of elements of 0.1-0.2 mm and three boundary layer prism layers with a total height of 0.05-0.15 mm. Careful mesh-dependency tests are necessary to achieve mesh-independent

solutions [49]. The presence vascular devices with very fine struts that are placed in vessels several order of magnitude larger in diameter pose a challenge to meshing algorithms. Computational meshes need to be computationally cost effective to solve for the flow in the aneurysm and parent arteries while, at the same time, be accurate enough to resolve the flow around the very thin wires of stents or coils and the near-wire grid elements must be fine enough to resolve the wires and accurately reconstruct flow through the implanted device. Stuhne and Steinman [50] suggested that the mesh resolution in the vicinity of the stent wires needs to be about one-third of the wires radius to achieve an accurate flow solution in the near-strut regions. Other studies (e.g., [51, 52]) have also reported on the properties of convergence of haemodynamics solutions in stented aneurysms with near-strut element sizes similar to what was reported by Stuhne and Steinman [50]. The widely-used body-fitted [53] grid generation can be complex and time-consuming for meshing aneurysms with implanted endovascular devices. Cebral et al. [54] proposed a hybrid method which uses the body-fitted approach to discretise the interior of the vessel walls but the adaptive embedded [53] approach for meshing the endovascular devices. Appanaboyina et al. [55] compared solutions produced by the hybrid approach and the pure body-fitted grids and showed their agreement (1-3% difference in predicting the maximum post-treatment velocity reduction over three predefined lines passing through the sac) after three levels of adaptive refinement of the near-strut elements in the hybrid approach.

Solving equations of motion requires setting the constitutive parameters (i.e., density and viscosity) as well as prescribing boundary conditions to the fluid. Blood flow in medium-sized arteries can be assumed to be incompressible with constant density. The rheology of blood can either be described by using a Newtonian model with a constant viscosity, which simplifies the equations of motion to the Navier-Stokes equations, or by using non-Newtonian models that consider the shear-thinning behaviour of blood.

As common practice in CFD modelling of blood flow in vascular domains, a velocity-related (usually flow rate) boundary condition is assigned at the inlet boundaries. This can be a constant flow rate (steady simulation) or a time-varying flow waveform (unsteady simulation). Such inflow boundary conditions are often derived from literature, where blood flow measurements are acquired in a particular artery for a specific cohort of people and reported in terms of descriptive statistics (mean values from standard deviations, see e.g. the works [56-58]). In some cases, patient-specific flow measurements are available from phase-contrast magnetic resonance imaging (PC-MRI) or Transcranial Doppler Ultrasound (TCD), patient-specific inflow boundary conditions are used for CFD simulations.

To prescribe outlet boundary conditions, zero-pressure boundary conditions are adequate for vascular domains with only one outlet. In contrast, in vascular domains with more than one outlet, flow distribution among outlet branches depends on the resistance and compliance of the distal vascular bed, which requires more advanced techniques to estimate the flow distribution ratio. However, many studies neglect the distal resistances and use zero-pressure outlet boundary conditions for multiple outlet vascular domains, which allows the flow to distribute among daughter branches according to their diameter and pressure drop[59]. To consider the effect of distal resistance and compliance, the three-dimensional computational vascular domain of interest can be coupled to lower-dimensional reduced-order models[60, 61]. However, although such boundary conditions give a more accurate representation of distal resistances, they increase the amount of parameters to be set in the model. Zero-dimensional (lumped parameter) [61, 62] models usually require setting the values of the terminal resistance and capacitance at each outlet branch. In one-dimensional models [63-66] the branching topology, length, diameter, and material properties of vessel segments need to be assigned. Although some studies (e.g. [67-69]) used fluid-structure-interaction techniques to account for

the arterial wall compliance in the models, wall distensibility is neglected in almost all CFD simulations of blood flow in aneurysms and a no-slip boundary condition is assigned on the walls.

Despite the use of various commercial or in-house solvers with different numerical solution strategies by CFD modellers for simulating aneurysmal flow, recent CFD challenges [70, 71] showed a global agreement between the haemodynamic quantifications produced by various CFD solvers in the participating groups. However, as noted, simulation of vascular blood flow requires proper setting of constitutive parameters and prescribing boundary conditions. Both constitutive parameters and boundary conditions are subject to intra-subject and inter-subject variabilities which introduce uncertainties into the computational models of blood flow. Intra-subject variabilities have roots in the state of the person (e.g., level of stress, physical activity, sleep pattern, etc.). For example, plasma volumes losses during maximal exercise will result in increases in haematocrit, haemoglobin concentration, and concentration of plasma proteins, which consequently increase the blood viscosity [72]. Inter-subject variabilities have roots in demographic characteristics (e.g., age, gender, weight, etc.) or the person's lifestyle (smoking, drinking, physical activity, etc.). For example, both aging and smoking will affect the arterial wall properties and consequently alter the arterial flow waveforms [58, 73]. On the other hand, uncertainties in computational blood flow simulations can also arise from assumptions associated to the underlying models (e.g., wall motion or blood rheological models). The influence of such uncertainties on the aneurysmal haemodynamics is discussed in the next section.

Uncertainty in blood flow modelling

Blood rheology is often assumed to be Newtonian, which while an acceptable approximation in medium-sized arteries, is strictly speaking not consistent with the shear-thinning nature of blood. An overestimation of aneurysmal WSS magnitude with almost no effect on the WSS distribution on the aneurysm sac has been reported in several studies comparing aneurysmal WSS values obtained from Newtonian and non-Newtonian simulations [13, 74, 75]. Xiang et al. [76] compared Newtonian CFD simulations with those performed with the Casson [77] and Herschel-Bulkley [77] models and observed almost similar WSS distributions and magnitude in two of the three examined aneurysms; in the other complex-shaped aneurysm, the Newtonian model overestimated WSS on the aneurysm bleb with a low WSS magnitude. Since low WSS regions are thought to be the regions where aneurysms may rupture, Xiang et al. [76] suggested that using a Newtonian model might underestimates the aneurysm rupture risk in aneurysms with pronounced low shear regions, e.g., complex aneurysm shapes with daughter aneurysms; they also noted the importance of blood rheology in simulating post-treatment flows where intra-aneurysmal stasis is induced in the presence of endovascular devices to trigger thrombosis and the aneurysm healing process. Castro et al. [78] compared CFD simulations performed with Newtonian and Casson models in ten multi-bleb aneurysms. They observed that the Casson model produced higher WSS values on some aneurysmal regions at some instances during the cardiac cycle. However, since the differences were not statistically significant, they concluded that there was no evidence that any of the models overestimate aneurysmal WSS values.

Gambaruto et al. [44] compared the effect of blood viscosity model and geometric uncertainties and showed that segmentation errors had greater effects on the model outcomes (errors in mean aneurysmal WSS were of order of 15% for geometric uncertainties and 5% for uncertainties in the rheological model). Fisher and Rossmann [79] compared aneurysmal WSS numerically predicted using four different rheological models in idealised aneurysm geometries; they showed that, compared to the parent vessel, the non-Newtonian effects were measurable inside the aneurysm sac (especially during the diastole); they observed the Carreau [77] model to be the most conservative, producing

lower WSS magnitudes with larger regions of low WSS. However, Fisher and Rossmann [79] emphasised that although the choice of the blood rheology model seems to have an effect on the numerical predictions WSS, the differences raised from uncertainties in the aneurysm morphology are still greater.

Other studies investigated the effect of blood rheological model in the presence of endovascular devices. Rayz et al. [25] investigated intra-aneurysmal haemodynamics in three fusiform aneurysms that were thrombus-free pre-treatment, but developed thrombus during follow-up studies. They showed a better agreement, although not statistically significant, between the low-flow regions and regions thrombus deposition when a non-Newtonian rheology was used. Morales et al. [80] studied the effect of blood rheology on steady flow simulations in three aneurysms before and after coiling; in untreated aneurysms, the Newtonian model overestimated intra-saccular velocities up to 16% in space-averaged velocities with a maximum of 45% in pointwise comparisons; these increased up to 55% in space-averaged velocities with a maximum of 700% in pointwise comparisons in coiled aneurysms; space-averaged WSS differed up to 2% and 12% between the two rheological models in the untreated and coiled aneurysms, respectively, while the Newtonian model overestimated the WSS in some cases and underestimated the WSS in others. These results demonstrate again the magnification of non-Newtonian effects in slow flow regions. However, Morales et al. [80] reported similar global flow patterns and post-treatment aneurysmal flow reductions in both Newtonian and non-Newtonian models. Admitting the observed magnitude differences in coiled aneurysms with thrombogenic slow flows, Morales et al. [80] concluded that a Newtonian rheology model could be adequate for blood flow simulations in coiled aneurysms, if the global haemodynamic alterations are used for device performance assessment. Huang et al. [81] studied the effect of blood rheology modelling choices in idealised stented aneurysms and observed that Newtonian models overestimated the intra-aneurysmal mean velocity magnitude by 6-26% in large-neck stented aneurysms and by 51-57% in small-neck stented aneurysms. Cavazzuti et al. [82, 83] investigated the effect of using a non-Newtonian rheology model in stented aneurysms and observed that average aneurysmal WSS values produced by the Newtonian rheology were around 15% greater in some regions and smaller in other regions; they concluded that the Newtonian to non-Newtonian effects are generally important but position dependent.

Among the above mentioned studies, Castro et al. [78], Morales et al. [84], and Fisher and Rossmann [79] performed quantitative comparisons between time-and-space-averaged aneurysmal WSS values obtained from CFD simulations based on Newtonian and non-Newtonian (Casson) rheology and reported values of time-and-space-averaged WSS on the aneurysm sac for different cases. According to a random-effects meta-analysis, the standardised mean difference (Hedges' *g*) was 0.02 with a 95% confidence interval of -0.04 to 0.07. This suggests limited effect of blood rheology model on WSS predictions by CFD. The meta-analysis based on these three studies failed to find a significant overall effect for the choice of rheological model (*p*-value = 0.292). None of the studies presented a pointwise comparison of aneurysmal WSS values provided by each rheology. Comparing time-and-space averaged WSS values, the study with the largest cohort performed by Castro et al. [78], showed that WSS values produced by Newtonian model were twice as large as the values predicted by non-Newtonian models at some aneurysmal regions; however, at some other regions on the same aneurysm, the Newtonian model predicted WSS values half as large as those predicted by the non-Newtonian model. They found no significant correlation between low WSS regions and regions where any of the models produced higher or lower WSS than the other.

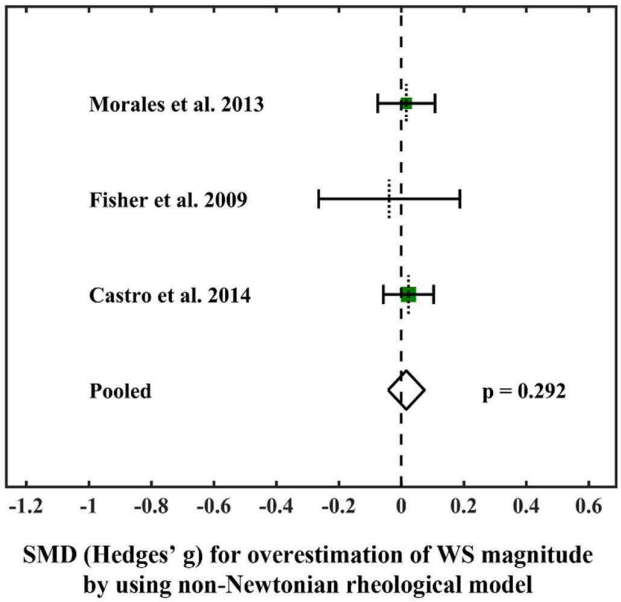

Figure 3. Forest plot showing the overestimation of space-and-time-averaged aneurysmal WSS produced by the non-Newtonian blood rheology. The plot illustrates effect sizes, Hedges' *g*, (represented by a square) and the confidence intervals (the horizontal lines) for each study and the pooled effect (the centre of the diamond) and its confidence interval (the width of the diamond) across all studies. Vertical dotted lines for each study show the study mean and the green squares are sized according to the study weight.

The forest plot presented in Figure 3 illustrates the results provided by the meta-analysis. Standardised mean differences (SMDs) , defined as the difference between the mean values of the two groups (i.e., Newtonian and non-Newtonian cases) divided by a representation of the standard deviation [29], are used to present effect sized reported by each study and the pooled effect size. Cohen's d and Hedges' g are two different formulations for calculation of the SDMs, which differ in the type of the standard deviation used to standardise the mean differences [29]. Since the Cohen's d is known to overestimate the effect sized in small samples [29], in this study we used Hedge's g which is the unbiased estimation of the effect size. As suggested by Cohen [85], effects of size 0.2, 0.5, and 0.8 can be interpreted as small, medium, and large, respectively. Based on the reviewed works and our meta-analysis, it can be concluded that differences between the aneurysmal WSS values produced by any of the investigated rheological models have not been shown to be significant. Although all the reviewed studies reported differences in magnitude of the WSS values, it is not still clear whether any of the investigated rheological models produce systematically larger or smaller WSS values. Flow stasis and low recirculating flow are known to play an important role in aneurysmal inflammatory phenotype and thrombosis, and consequently in rupture or device-induced aneurysm healing. Thus, the observed discrepancies in WSS values suggest consideration of non-Newtonian behaviour of blood where the aneurysmal flow is very slow and disturbed due to the irregular aneurysm shape or is reduced by endovascular devices. Such consideration is more important when local haemodynamic evaluations, rather than global time- or space-averaged haemodynamic quantities, are of interest. Moreover, although all the reviewed studies reported almost no influence of blood rheological model on the WSS distribution and characterisation of regions where shear stress is relatively low or high, it is not still clear whether the reported discrepancies in magnitude and direction of CFD-predicted shear stresses result in false predictions about the aneurysm or the endovascular treatment fate.

Inlet boundary conditions to the vascular model of interest are another ingredient of the flow simulation that contains uncertainty. Inflow boundary conditions are often taken from literature, where typical flow waveforms in a particular artery are reported for a specific cohort of people who usually have demographic differences with the specific patient whose aneurysm is being simulated. Some studies [86-88] used patient-specific inflow boundary conditions obtained from patient-specific measurements. Such patient-specific boundary conditions are superior to the typical literature-based boundary conditions, since they are acquired from the same patient. However, even the patient-specific boundary conditions cannot fully represent systemic blood flow, since systemic flow is highly dependent of the state of the person (e.g., level of stress, physical activity, sleep pattern, etc.) and measurements are only acquired at a particular point in time and under very specific scanning conditions. Nevertheless, although not representative of the effect of intra-subject variability, using one-shot measurements of patient-specific inflow boundary conditions has been shown to have limited effects on the distribution of WSS and OSI on the aneurysmal sac. However, comparing results obtained from simulations with typical literature-based and directly measured inflow boundary conditions has revealed remarkable differences in the magnitude of aneurysmal WSS and OSI [86-89]. Consequently, exactly how intra-/inter-subject variations of systemic flow conditions may affect intra-aneurysmal haemodynamics and the rupture risk has become a relevant question within the research community.

Bowker et al. [90] investigated the effect of moderate aerobic exercise on three middle cerebral artery aneurysms and observed an average of 20% increase in time-averaged WSS on the aneurysm sac; this result has been obtained by keeping the inlet waveform fixed and increasing the time-averaged inflow and heart rate by 7.8% and 73.4%, respectively. Geers et al. [91] systematically investigated the effect of time-averaged inflow rate, heart rate, and inflow wave pulsatility index and showed that, under a fixed time-averaged flow rate, increasing heart rate and inflow pulsatility index had no effect on the aneurysmal time-averaged WSS magnitude. Xiang et al. [92] studied the effect of inflow waveforms on intra-aneurysmal haemodynamics of four aneurysms. They performed CFD simulations with four different waveforms that had the same time-averaged flow rate and showed that different waveforms produced the same spatial distributions on WSS and oscillatory shear index (OSI) on the aneurysm wall. They also observed the same values of time-averaged WSS magnitudes, but drastically different values of OSI in the four CFD simulations performed for each aneurysm. They finally concluded that inflow boundary conditions have only limited effects on the aneurysmal WSS and OSI for the purpose of aneurysm rupture stratification. Keeping the time-averaged flow rate fixed, Sarrami-Foroushani et al. [93], performed CFD simulations using inflow waveforms obtained from a data-driven model of internal carotid artery flow and observed that variations in ICA flow waveform had no effect on the time-averaged WSS but altered the local directionality of WSS; they also showed that the inflow waveform variations changed the rupture outcome prediction in 4 out of 19 cases when simple logistic regression model was used to predict the rupture outcome. For each aneurysm in a fifteen-aneurysm cohort, Morales et al. [84] performed eleven CFD simulations with different inflow rates (but using the same waveform) and showed that spatiotemporally averaged aneurysmal WSS varied as a quadratic function of time-averaged inlet flow rate. They showed that values of aneurysmal OSI did not change by changing the time-averaged flow rate while keeping the waveform constant.

Since patient-specific flow measurements are rarely available as a clinical routine for aneurysm patients, CFD modellers often scale the typical literature-driven flow waveforms to approximately impose patient-specific boundary conditions to their models. For each aneurysm model, scaling is performed in order to maintain a fixed spatiotemporally averaged velocity or WSS at the inlet boundary. The literature-based flow rate is scaled according to the inlet diameter squared, if the scaling is based on time-and-space-averaged velocity, and cubed, if the scaling is based on time-and-

space averaged WSS. The choice of inlet location (and consequently inlet diameter) and scaling model (cubed or squared) is, however, a source of uncertainty in inlet boundary conditions. Valen-Sendstad et al. [94] investigated the effect of the choice of inlet location and the scaling model on the resulting inflow rates. They showed that scaling according to the squared diameter produced flow rates more consistent with the physiological flow rates. They also quantified the uncertainties arising from truncating the ICA at different locations and showed that all truncation locations below the cavernous segment produced the same uncertainties as physiological uncertainties of ICA flow rate and thus lead to reliable CFD simulations. Visually comparing CFD-predicted and DSA-imaged intra-aneurysmal flow patterns, Pereira et al. [95] showed that reliable CFD outcomes were obtained using vascular models with inlet vessels truncated as far upstream as obtainable from the medical images, and coupled to Womersley inlet velocity profiles. Hodis et al. [96] also studied the effect of inlet artery length on 10 ICA ophthalmic aneurysm models and showed that removing two bends from the parent artery resulted in approximately 15% error in peak systolic space-averaged WSS over the aneurysm sac.

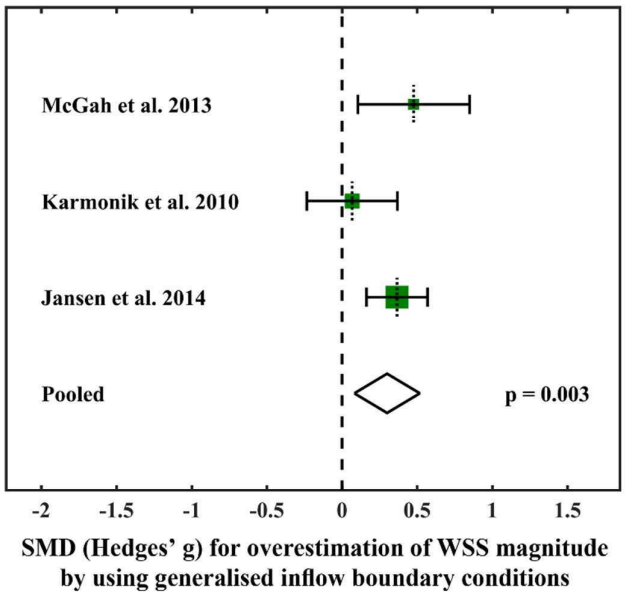

Figure 4. Forest plot showing the overestimation of space-and-time-averaged aneurysmal WSS produced by the generalised inflow boundary conditions. The plot illustrates effect sizes, Hedges' g, (represented by a square) and the confidence intervals (the horizontal lines) for each study and the pooled effect (the centre of the diamond) and its confidence interval (the width of the diamond) across all studies. Vertical dotted lines for each study show the study mean and the green squares are sized according to the study weight.

Jansen et al. [86], McGah et al. [88], and Karmonik et al. [89], performed quantitative comparisons between time-and-space-averaged aneurysmal WSS values obtained from CFD simulations based on measured patient-specific and generalised inflow boundary conditions and reported values of time-and-space-averaged WSS on the aneurysm sac for different cases. In these studies, the inlet boundaries of the vascular domains located on the internal carotid artery (ICA) and generalised ICA flow waveforms were obtained from studies by Ford et al. [56] and van Ooij et al. [97], in which the ICA flow was measured over cohorts of 17 young and healthy volunteers and 8 patients with intracranial aneurysms, respectively. For each aneurysm case, McGah et al. [88] scaled the generalised waveform to maintain a physiological mean WSS of 1.5 Pa at the inlet boundary. However, Karmonik et al. [89] directly used the generalised flow waveforms obtained from the study by Ford et al. [56] without scaling; while Jansen et al. [86] have not reported the scaling process clearly. According to a random-effects meta-analysis, the standardised mean difference (Hedges' *g*) was 0.30 with a 95% confidence

interval of 0.08 to 0.52 (p-value = 0.003). This suggests a moderate effect of inflow waveform on the prediction of WSS magnitude by CFD. Figure 4 illustrates the results provided by the meta-analysis of the effect of using generalised boundary conditions on the aneurysmal WSS magnitude. It is worth noting that in this meta-analysis study, we used aneurysmal WSS values provided by patient-specific boundary conditions as the baseline values. WSS values generated by the generalised boundary conditions can be arbitrarily higher or lower than the baseline values. However, we calculated the effect sizes in a consistent way keeping the WSS values generated by patient-specific boundary conditions as baseline for all studies. Thus, bearing in mind that the "sign" has no physical meaning in this meta-analysis, the term "overestimation" was used in consistency with other meta-analyses presented in this work.

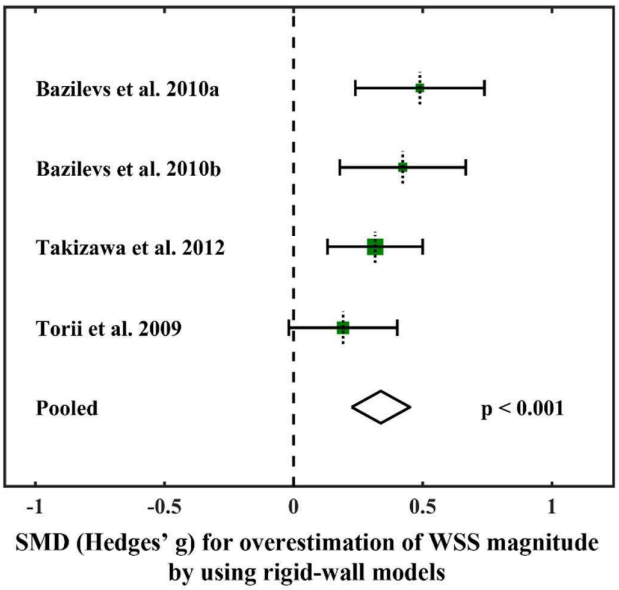

Figure 5. Forest plot showing the overestimation of maximum peak systolic aneurysmal WSS produced by the rigid arterial wall assumption. The plot illustrates effect sizes, Hedges' g, (represented by a square) and the confidence intervals (the horizontal lines) for each study and the pooled effect (the centre of the diamond) and its confidence interval (the width of the diamond) across all studies. Vertical dotted lines for each study show the study mean and the green squares are sized according to the study weight.

A rigid-wall assumption is often made in cerebrovascular blood flow simulations [98]. Estimating regional aneurysmal wall motion from dynamic X-ray images, Dempre-Marco et al. [67] compared CFD simulations of blood flow in aneurysms with rigid and non-rigid wall assumptions and observed that, although the distribution of WSS on the sac and elevated WSS areas remained almost identical, rigid wall simulations tended to overestimate the pointwise aneurysmal WSS magnitude by around 50%. On the other hand, fluid-structure-interaction (FSI) techniques have been used to simulate aneurysmal flow in non-rigid aneurysmal models. Torii et al. [68, 69, 99] performed non-rigid fluid-structure-interaction simulations on aneurysms and reported up to 20% differences among WSS magnitudes obtained from rigid and non-rigid simulations. Takizawa et al. [100], Bazilevs et al. [101, 102], and Torii et al. [99], performed quantitative comparisons between maximum peak systolic aneurysmal WSS values obtained from rigid and flexible wall (fluid structure interaction) CFD simulations and reported values of time-and-space-averaged WSS on the aneurysm sac for different cases. According to a random-effects meta-analysis, the standardised mean difference (Hedges' g) was 0.34 with a 95% confidence interval of 0.22 to 0.45 (p-value < 0.001). Figure 5 illustrates the results provided by the meta-analysis.

Our meta-analysis suggests an effect of wall distensibility on the prediction of WSS magnitude by CFD. However, visual inspections and quantitative comparisons based on global space-averaged measures showed an agreement between the rigid-wall and non-rigid-wall simulations as long as the distribution of WSS on the aneurysm wall, or the main characteristics of flow in the aneurysm (e.g., the complexity of flow pattern, or presence of an impinging flow jet, etc.) are of interest [13, 67, 103]. The main challenge to the current structural models of aneurysm wall is the present limitations in measurement techniques leading to uncertainties in identification of wall mechanical properties like thickness or modulus of elasticity. Aneurysms often have pathological walls with material properties varying spatially over sac. Despite some attempts to create ad hoc models of such variations, e.g. a thinner wall on the sac [104], the structural models are still far from the physiological reality. Thus, notwithstanding the important effects induced by rigid wall assumption, such issues with realistic quantification of aneurysm wall mechanics have resulted in rigid-wall CFD simulations remaining predominant in the context of intracranial aneurysm modelling. To the best of our knowledge, the effect of using rigid-wall assumption on rupture risk stratifications and predictions of endovascular treatments' outcome has not been studied yet. However, the observed effects on WSS magnitudes, and presumably direction, magnifies the importance of future studies on non-rigid aneurysm wall models, especially when quantification of WSS and its mechanistic relation to the aneurysm wall biology and intra-aneurysmal thrombogenesis is of interest, e.g., in VETMs.

All in all, our meta-analyses found that wall distensibility and inlet flow waveform uncertainties have effects on the magnitude of aneurysmal wall shear stress predictions by CFD. Since only the maximum WSS values, representing a state of maximum stress [105] and wall deformation [101], were reported in some of the studies, our meta-analysis on the effect of wall distensibility is based on maximum WSS. This limits the comparability of wall compliance meta-analysis with the other two meta-analyses that are based on the averaged WSS, i.e., the meta-analyses on the effect of inflow waveform and blood rheology. In future, in order to perform compliant wall simulations, improvements on the structural models of arteries and current techniques for measuring mechanical properties of the aneurysm wall are necessary. To the best of our knowledge, the effect of rigid wall assumption on the *endovascular treatment predictions*, and *stratification* and *rupture risk assessment* of intracranial aneurysms has not been explored yet. In addition, inter-subject variability of arterial flow rates as well as intra-subject variations of the systemic flow conditions in response to the regulatory systems lead to an uncertainty in the parent arteries' flow rate waveforms. Despite the recent studies [92, 93] on quantification of the uncertainties raised from inter-subject variability of inflow waveforms, the effect of intra-subject variability of systemic flow on aneurysmal WSS is still not attempted by the research community. Recent studies [106, 107] have revealed some new aspects of the effect of flow multi-directionality on the biological responses of the endothelium, which may play an important role in aneurysmal wall inflammation and degradation and aneurysm thrombosis by activating platelet activators [108, 109]. However, the sensitivity of WSS directionality to the above mentioned sources of uncertainty has not been well investigated in the literature. These, on the other hand, accentuate the importance of addressing geometric and flow uncertainties in the endovascular treatment models.

Uncertainties in aneurysmal blood flow modelling may also arise in outlet boundary conditions. Ramalho et al. [110] investigated the sensitivity of intra-aneurysmal haemodynamics to the outlet boundary conditions assigned using four different methods: traction-free, zero-pressure, coupling to a zero-dimensional model, and coupling to a one-dimensional model. They observed that coupling the outlet boundary to a zero-dimensional or a one-dimensional model resulted in more appropriate flow distribution between the side branches. However, using the reduced-order models as boundary conditions requires proper choice of model parameters, like resistance and capacitance in zero-dimensional models, and vascular structural and mechanical properties in one-dimensional models.

Uncertainty in such model parameters should be addressed to produce reliable patient-specific results, e.g. [111, 112].

In addition to the uncertainties in quantifying physiological model parameters (i.e., blood density and viscosity) and boundary conditions, variabilities in discretisation strategies may influence the model outcomes. Providing a fixed set of boundary conditions and flow model parameters, the two recent CFD challenges on aneurysmal flow modelling invited CFD modellers to simulate blood flow in selected aneurysms and investigated how variations in solution strategies influence aneurysmal blood velocity and pressure quantifications. In the Aneurysm CFD Challenge 2013 [113], despite using different solution strategies and resolutions (mesh sizes of 86k-31200k using first or second order elements and time step sizes of 0.01-10 ms), approximately 80% of the 26 participating groups reported similar results with standard deviations of below 9% for cycle-averaged and peak systolic velocity, and pressure on the parent artery centreline in the two aneurysm cases studied; flow inside both studied aneurysms was stable and comparison among participating groups resulted in standard deviations below 20% for the velocity cut-planes through the aneurysm sacs. However, the aneurysmal flow inside the aneurysm involved in the Aneurysm CFD Challenge 2012 [71] was not stable and thus despite the overall agreement among the 27 submitted solutions, solutions with higher temporal resolutions (time step sizes below 0.2 ms) were able to capture flow instabilities; detection of flow instabilities by some groups resulted in greater inter-study variabilities particularly in peak systolic velocity patterns. According to the above challenges, CFD simulations with high temporal resolutions of at least 0.2 ms are required to capture aneurysmal flow instabilities. On the other hand, despite a strong correlation ($R^2 > 0.9$) between time-averaged WSS magnitudes, Valen-Sendstad et al. [114] observed a weak correlation ($R^2 = 0.23$) between OSI values predicted by normal (with spatial resolutions of 0.1-0.2 mm and temporal resolutions of about 1 ms) and high resolution (with spatial resolutions of about 0.06 mm and temporal resolutions of about 0.05 ms) simulations. Comparing normal and high resolution CFD simulations, they observed an average of 30% and 60% differences in pointwise values of time-averaged and maximum WSS on the aneurysm sac, respectively. They suggested that particularly for bifurcation unstable aneurysms, normal resolution CFD simulations cannot accurately capture oscillations both in magnitude and direction of WSS vectors. Due to the observed differences between OSI values and pointwise WSS magnitudes predicted by normal and high resolution schemes, Valen-Sendstad et al.[114] argued that although normal resolution CFD simulations may be adequate for aneurysm rupture risk assessment based on spatiotemporally averaged flow indices, they cannot be relied on to fully characterise WSS as a complex biomechanical stimuli on the aneurysm wall.

Mesh resolution near the wires also influences the flow quantification in the presence of endovascular devices. Comparing the solutions provided by 6 participating groups for three particular stented aneurysms, the Virtual Intracranial Stenting Challenge (VISC) in 2007 [70] showed that an accurate reconstruction of blood flow around the stent wires requires an adequately fine mesh resolution near the struts. Janiga et al. [48] observed more than 15% relative difference between intra-aneurysmal maximum flow velocities obtained based on first- and second-order numerical discretisation. They recommended second-order solvers for flow simulation in stented aneurysms.

To sum up, mesh-dependency tests are necessary when building VETMs, in particular, to ensure the convergence on the aneurysmal wall and near the device wires. Although assessments of device performance based on the highly reduced indices (e.g., flow reduction or increase in the aneurysm sac turnover time) can be done using coarser discretisations, higher resolution CFD simulations are required for an accurate resolution of velocity and WSS fields, especially when the interaction between localised haemodynamics and biology is of interest, e.g., platelet activation in the high shear flows between the struts [22], and inflammatory or thrombogenic biochemical surface reactions

[107, 115]. In VETMs, CFD solutions require temporal resolutions higher than 0.2 ms to capture flow instabilities of interest, and spatial resolutions in the order of 0.1-0.2 mm within the vasculature and of about one-third of the wire radius near the wires. In addition, volumetric meshes require at least a few layers of prismatic boundary layer elements near the wall.

Modelling of endovascular devices and their deployment

Mathematical models developed for device deployment can be either mechanistic (physics-based) or phenomenological. Mechanistic models of device deployment dynamics account for the design and mechanical properties of the particular device and its mechanical interactions (contact) with the flow, the arterial wall, and the device itself. This makes mechanistic models potentially more accurate. However, such models have a large number of model parameters and, consequently, are more prone to uncertainty in the identification of model parameters. In contrast, while they may ignore some of the underlying biomechanical mechanisms, phenomenological models make certain geometrical or physical assumptions to describe the observable process of device deployment. These models are computationally faster and their parameters are more easily obtainable from the device manufacturer. Therefore, phenomenological models are more commonly used for simulating virtual treatment procedures for the embolisation of aneurysms.

Mechanistic virtual coil models have been employed to describe the dynamics of coil deformation after insertion into the aneurysm sac [116-119]. Such models may have many ingredients to adjust in order to optimise the deployment strategy, such as the diameter, length, and mechanical properties of the coils as well as a proper set of boundary conditions describing interactions of the coil with the micro-catheter, aneurysm wall, and the coil itself. Equations of blood flow are then solved within the coiled aneurysm. Phenomenological models of endovascular coil deployment can be categorised into: (i) models that only modify the governing equations of blood flow to account for the impedance of fluid flow in the porous region of a thrombosed coil [120-124], and (ii) models that use mathematical descriptions to explicitly model the coil deployment inside a specific aneurysm and then solve blood flow equations in the aneurysm sac with a deployed coil inside [54, 125-127]. The dynamics of stent deployment have been mechanistically modelled using finite element models (FEMs) [11, 128-131]. Such models, however, are very computationally expensive since they consider the structural properties of the stent as well as its interactions with the micro-catheter and the vascular wall. Phenomenological models describe the endovascular stent by representing it as a porous medium [132, 133], by mapping of the stent design on a previously expanded cylinder inside the vessel [54, 55], by deforming a mesh until it reaches the vessel wall [10, 52, 134, 135], or by weaving stent wires around a circular cone deformed to fit against the vessel wall [9]. Flore et al. [130] and Bernardini et al. [128] compared aneurysmal flow after placement of an endovascular stent with a mechanistic FE model with that predicted after deploying the stent using a phenomenological fast virtual deployment model and observed a good quantitative agreement accompanied by a reduction in the computational time.

Virtual treatment models have been used to pre-operatively study the effect of coil shape, orientation, and packing density in patient-specific aneurysm models. Schirmer et al. [127] investigated the effect of orientation of helical coils on the aneurysmal flow and showed that the coil orientation with respect to the aneurysmal flow has a considerable influence of the effectiveness of helical coils. They showed that helical coils that are located parallel to the flow jet entering the aneurysm are more effective in preventing flow from entering the aneurysm and reducing the level of aneurysmal WSS. They observed the least flow reduction in aneurysms with coils placed orthogonal to the entering jet. Similarly, Jeong et al. [136] investigated the effect of coil shape and orientation on the aneurysmal haemodynamics and showed that cage-shaped coils deployed orthogonally to the

entering flow jet provided the least flow reduction in aneurysms. Aguilar et al. [137] studied the effect of coil surface area (diameter) and packing density on the intra-aneurysmal flow. They observed that coiled aneurysms with the same coil surface area but different packing densities produced similar intra-aneurysmal haemodynamics. They also observed that the coiled aneurysm with the largest coil surface area had the most effect on flow reduction and concluded that the coil surface area influenced on its performance. Morales et al. [138] studied the effect of coil packing density and configuration on the intra-aneurysmal flow and showed that at low packing densities (< 12%), the aneurysmal flow was highly dependent on the coil configuration and this dependency decreased as packing density grew. They observed an insignificant influence of coil configuration at high packing densities.

Aneurysmal haemodynamics following the placement of a flow diverter stent are known to be dependent on the aneurysm size and shape [139-142], location [139, 141], stent design and configuration [129, 135, 143-146], and its orientation and position in the parent vessel [147-150]. The stent porosity has also been shown to highly influence the effectiveness of the deployed stent [151, 152]. Virtual treatment models provide the opportunity to investigate the effect of the aforementioned variables using image-based patient specific models before the actual placement of flow diverters [15]. In clinical practice, flow diverters are usually selected to be oversized, i.e., to have slightly greater diameter than the vascular calibre. This results in an adequate appositioning against the vascular wall on the one hand and a stretch of stent cells along the vascular axis on the other. Mut et al. [153] studied the effect of stent oversizing on the post-treatment aneurysmal haemodynamics and showed that oversizing will result in larger stent cells and will decrease the haemodynamic effectiveness of the flow diverter stent. While deploying flow diverters, clinicians can maximise the strut local compaction, and consequently the flow diversion, across the aneurysm neck. The dynamic push-pull flow diverter deployment technique has been used to increase and decrease the local density of the flow diverter at the aneurysm neck and perforator-rich regions of the parent vessel, respectively, to allow maximum flow diversion at the neck while maintaining the perforators and branch vessels [154]. Janiga et al. [155] simulated flow through similar flow diverters that are differently deployed to have eight different local compactions at the neck; and, observed that different local compactions lead to different post-deployment intra-aneurysmal flow reductions ranging from 24.4% to 33.4%. They remarked that flow diverter local compaction across the aneurysm neck can be virtually and pre-operatively optimised to reach maximum flow reduction. However, Xiang et al. [22] simulated this deployment technique and showed that although resulting in an increased flow diversion, it pushes the flow diverter to bulge out inside the aneurysm, and produces a weaker inflow compared to the standard deployment technique that results in lower shear rates near the stent struts. Since high shear-induced activation of platelets plays a role generation of a stable white thrombus (versus instable stasis-induced red thrombus) inside the aneurysms, Xiang et al. [22] suggested that this deployment technique may result in lowering the platelet activation and, consequently, white thrombus formation potential.

Performance of endovascular devices in treatment of aneurysms is assessed by their ability to induce a flow stasis and consequently an occluding stable blood clot in the aneurysm sac [2]. Virtual endovascular treatment models can be used to pre-operatively predict the likelihood of recanalisation in candidate aneurysms for coil embolisation. Presence of high WSS (> 35 Pa as reported by [156, 157]) at the neck of the coiled aneurysms was shown to have a correlation with post-treatment recanalisation and regions of high WSS coincided with regions where recanalisation happened [156-159].

Delayed or incomplete occlusion and post-treatment rupture are the challenging complications associated with flow diverter treatments. Currently, there is no reliable measure to predict the

performance of implanted flow diverters in terms of inducing a durable clot that occludes the sac completely and triggers the process of healing. Several attempts have been made to computationally quantify the stent-induced post-treatment haemodynamic alterations and use them to predict the treatment outcomes. Chung et al. [160] evaluated the treatment outcome in 36 rabbits with elastase-induced aneurysms treated with flow diverters; nine aneurysms were occluded completely or near completely within 4 weeks (categorised as *fast* group) and six aneurysms incompletely occluded at 8 weeks (categorised as *slow* group); differences were observed between the morphological indices of the two groups; e.g., neck area was 0.365±0.082 cm^2 in the slow and 0.144 ±0.078 cm^2 in the fast occlusion group, p-value = 0.015. However, from haemodynamic measures (measured immediately after stent deployment), the aneurysm inflow rate and mean intra-aneurysmal velocity were lower in the fast occlusion group (inflow rate was 0.155±0.095 mL/s in the slow and 0.047±0.053 mL/s in the fast occlusion group, p-value = 0.024 and intra-aneurysmal velocity was 0.506±0.298 cm/s in the slow and 0.221±0.224 cm/s in the fast occlusion group, p-value = 0.058); no differences were observed between WSS-based measures (e.g., space-averaged WSS, minimum WSS, or low WSS areas). Mut et al. [161] examined post-stent aneurysm flow in 23 aneurysms (15 aneurysms considered as *fast* with occlusion times less than 3 months, and the other 8 considered as *slow* with incomplete occlusion or patency at 6 months); they found differences in post-treatment mean velocity (1.89±1.88 mL/s in the slow and 0.47±0.52 mL/s in the fast group, p-value = 0.021), inflow rate (3.11±2.04 cm/s in the slow and 1.13±0.92 cm/s in the fast group, p-value = 0.004), and shear rate (32.37±20.93 /s in the slow and 20.52±23.18 /s in the fast group, p-value = 0.021) values between the fast and slow groups; they suggested a threshold of 1.3 cm/s on post-stent mean velocity could predict occlusion time (slow or fast) with an accuracy of 84%. Kulcsar et al. [162] examined pre- and post-treatment haemodynamics in eight para-ophthalmic aneurysms treated with flow diverters; one was occluded but ruptured 5 day after treatment, one remained patent after one year, and others were occluded during the one year follow-up. In aneurysms with complete occlusion, they observed reductions of 10%-80% in the mean velocity, 12%-58% in the maximum velocity, 44%-81% in the mean WSS, and 32%-82% in the maximum WSS after flow diverter placement; however, mean and maximum velocities, and mean and maximum WSS were reduced by 60% and 47%, and 68% and 60% in the aneurysm that remained patent, respectively. In the aneurysm with post-treatment rupture, Kulcsar et al. [162] also observed 20% and 0% reductions in the mean and maximum velocities, respectively, while the mean WSS was reduced by 60% and a reduction of 20% was observed in the maximum WSS after stenting. They pointed out that lower reduction rate in the maximum velocity of the ruptured aneurysm suggest a persisting jet that prevent the successful occlusion of this aneurysm. However, based on the observations reported by Kulcsar et al. [162], the averaged haemodynamic measures in the case with persisting patency are not significantly different from those aneurysms with successful occlusion. Focusing on the relative changes (post- to pre-treatment ratio) induced by flow diverters, Ouared et al. [163] attempted to find patient-unspecific haemodynamic ratio thresholds that significantly determine the condition required for a durable aneurysm occlusion; they examined pre- and post-stent space-and-time-averaged velocity and WSS in 12 aneurysms (nine were occluded at 12 months' follow-up while the remaining three were still patent) but found no significant absolute occlusion threshold based on post-stent velocity and WSS absolute values; however, they found an area under curve (AUC) with a p-value of only 0.052 for pre- to post-stent mean velocity ratio with a minimum of one-third velocity reduction necessary to generate a long-term occlusion (with a sensitivity and specificity of about 99% and 67%, respectively), independent of the aneurysm geometry; despite post-treatment WSS reductions in all aneurysms, they could not find any significant occlusion threshold based on post- to pre-stent WSS ratios.

The above-mentioned studies identified reductions in aneurysmal flow and WSS following the treatment with endovascular devices; however, most of them found no significant haemodynamic

differences between cases with successful occlusions or persisting patency. Although the observed post-treatment haemodynamic changes suggest the capability of pure haemodynamic models in predicting the treatment outcomes, the limited sample sizes in each individual study prevents any general conclusion; for example, all aneurysms included in the study by Kulcsar et al. [162] have post-treatment mean velocities greater than what is suggested by Mut et al. [161] as a fast occlusion threshold; or the so called patient-unspecific velocity reduction occlusion threshold proposed by Ouared et al. [163] results in a sensitivity and specificity of about 67% and 50% in the cohort studied by Kulcsar et al. [162]. Despite the important role of WSS on aneurysm wall biology and initiation of thrombosis, none of the reviewed studied identified a significant difference between the fast and slow occlusion outcomes based on averaged WSS-based measures; this could be attributed to the highly localised patterns of aneurysmal WSS and the consequent biological aneurysm wall phenotypes that are captured by the averaged quantities studied in the mentioned works. Moreover, inducing a selective aneurysmal clotting that triggers the healing process is crucial [164]. Unlike the stasis-induced red thrombus, which is less organised and contains a high content of leukocytes and proteolytic enzymes, white thrombus is more stable and contains a low content of leukocytes and proteolytic enzymes [22]. Unstable red thrombus forms under low shear flow; conversely, white thrombus forms through activation of platelets in high shear rate regions (e.g., near the stent struts) [22]. Recent findings on post-procedural ruptures of aneurysms treated with flow diverters suggest that the presence of fresh and non-organised red thrombus may result in a pathophysiological cascade leading to aneurysm wall degradation and rupture [21]. This revealed that device-induced intra-aneurysmal flow stasis may result in formation of unorganised red thrombus and lead to aneurysm rupture after treatment. Xiang et al. [22] hypothesised that white thrombus should desirably be induced in the aneurysm to promote stabilisation red thrombus and generate a stable clot that assist in the formation of a neointimal layer over the aneurysm neck. The hypothesis that the stable intra-aneurysmal clot is a combination of red (forms via stent-induced stasis) and white (forms via stent-induced platelet activation) thrombi needs further investigation and validation [22]. This hypothesis also magnifies the importance of appropriate anticoagulant/antiplatelet therapies in such complex problems [22, 164]. Summing up, the favourable treatment outcome, i.e., formation of a complete stable clot at a rate faster than thrombus-induced wall degradation, however, is highly affected by the mechanical and biochemical interactions between clot and intra-aneurysmal flow, in the presence of the anticoagulant/antiplatelet therapies. The above discussion implies that whether or not an implanted endovascular device leads to a complete aneurysm occlusion may not be assessed only based on post-treatment highly averaged haemodynamic quantities. *Information* from the intra-aneurysmal biochemistry and biology is required to reliably predict device performance. This could be achieved by coupling mechanistic blood coagulation sub-models to the VETMs or devising more advanced phenomenological haemodynamic surrogates that capture the ongoing biological processes more effectively. Creating *device performance indicators* that compare the device-induced formation rates of instable red versus stable white thrombi in the presence of anticoagulant/antiplatelet therapies may help predict the efficacy of an endovascular device for a specific patient.

Uncertainty in modelling of the endovascular devices

Uncertainty in modelling of the endovascular devices can arise either from uncertain model parameters or the way each model represents deployment of the device and its interaction with blood flow (model uncertainty). Phenomenological models of coil and stent deployment often rely on parameters such as device design, diameter, and length, which are often obtainable from the manufacturer. However, mechanistic models include mechanical properties of the devices and boundary conditions, which cannot be easily measured, and thus, introduce uncertainty into the model. The effect of device configuration, orientation, and position of the devices has been

investigated in the literature, but to the best of our knowledge, the quantification of the uncertainty in the model parameters has not been attempted so far.

Modelling endovascular devices as porous media, although is not strictly a source of uncertainty, introduces errors in quantification of aneurysmal flow; especially local values of haemodynamic variables. Morales et al. [12] compared post-treatment aneurysmal flow fields obtained from modelling the deployed coil as a porous medium with that obtained from modelling the coils explicitly. They observed considerable differences in intra-aneurysmal velocity and local concentration of contrast agent predicted by each of the two techniques. However, due to the lack of quantitative comparisons between post-treatment aneurysmal flow fields obtained from models and in vivo measurements, it is not yet certain, which of the proposed models better represents the device performance under specific conditions. Levitt et al. [165] compared post-treatment haemodynamics in two coiled aneurysm phantoms numerically simulated using the porous medium technique and explicit model of coils obtained from high-resolution high-energy synchrotron X-ray micro-tomography; substantial differences up to 50% and 130% respectively in time-averaged WSS and OSI values averaged over the aneurysm sacs suggest inaccurate haemodynamic quantifications using homogeneous porous medium coil models. Although synchrotron tomography is not currently available in the routine clinical practice, this modality can be used to evaluate the accuracy of other more complex coil modelling techniques. In two of the three stented aneurysms, Raschi et al. [166] reported a qualitative and quantitative agreement (with up to 10% difference in post-treatment reductions in aneurysm-averaged WSS) between aneurysmal post-treatment haemodynamics predicted by explicit and porous medium models of the deployed stents; in the third aneurysm, post-treatment reduction in aneurysm averaged WSS differed up to 25% between the porous medium and explicit models of the flow diverters. In a similar study with two stented aneurysms, identical WSS distributions with relative root mean square errors of 21%-24% in mean WSS magnitude averaged over the entire sac and 45%-81% in mean WSS magnitude averaged over the aneurysm dome are reported for simulations with flow diverters modelled either as porous medium or explicitly [132]. Capturing the local variations of porosity is a challenge in porous medium models of both coils and flow diverters. For example, complex geometry of the host artery, or particular deployment techniques (e.g., the push-pull technique) result in local variation of stent porosity at the aneurysm neck which cannot be easily mimicked by the porous medium models; especially if pre-operative evaluations of the devices are of interest so that the post-deployment porosities cannot be estimated by micro-tomography techniques. Thus, although refinements may improve on the predictions by encouragingly cost-effective porous medium models, the geometrical complexity of endovascular devices and the consequent effects on the flow seem to be a serious challenge to these models.

Intra-procedural changes in the host vessel geometry (shape and size) introduce further uncertainties in VETMs that has yet to be studied in more detail and quantified. The parent vessel can undergo dilation as a consequence of stent expansion during deployment, vasodilator drug administration, and the intentional post-release manipulations to correct stent apposition all leading to reported differences of about 5% and 10%, respectively, between virtual and real stent final radius and length [167]. Delayed geometrical and angular alterations of the host arteries within a year after deployment are also reported in stented aneurysms [168]. Straightening of the parent artery after deployment of stents was reported by King et al. [169] In sidewall vertebral artery aneurysms, this resulted in alterations in the flow direction and rate (by 10%) of the aneurysm inflow jet [170]. However, none of the current deployment techniques accounted for such device-induced geometrical alterations [48]. Formation of a rapid and stable clot, which completely occludes the aneurysm sac, is the desired goal of a successful endovascular aneurysm treatment [171]; and, uncertain intra-procedural alterations in the physiological flow can affect the treatment outcome.

Mut et al. [172] investigated intra-aneurysmal haemodynamics in aneurysms treated with three different stents under five different time-averaged flow rates in the parent vessel and observed that a change of 30-50% in the parent vessel flow rate during the stenting procedure resulted in a 30-80% change in the aneurysmal haemodynamic variables. This observation highlights the importance of inlet flow variability as a source of uncertainty (see the uncertainty in blood flow modelling section) in vascular treatment models.

Modelling blood clotting

Clotting in aneurysms

In ruptured intracranial aneurysms, clot formation is the response of the haemostatic system and prevents blood loss at the site of injury, where the aneurysm has burst. Chronic spontaneous thrombosis can also occur in unruptured aneurysms, resulting in further wall damage and later aneurysm rupture or a natural healing process through complete occlusion of the aneurysm sac [173]. On the other hand, as mentioned before, intrasaccular thrombosis can also be induced by endovascular devices, like coils and stents, to occlude aneurysm sac from the vascular bed and reduce the rupture risk.

The desired process of healing in endovascular treatment is to generate a stable clot throughout the aneurysm sac. The aneurysm will then be excluded from the parent vessel by formation of a neointimal layer over the aneurysm neck [174-176]. Endovascular treatments are associated with complications such as incomplete occlusion, recanalisation or recurrence [177, 178], and thromboembolisation [179], which expose the patient to the risk of a later haemorrhage or an ischemic stroke. Anticoagulant drugs are usually prescribed after endovascular treatments [180], and prevent uncontrolled acute device-induced thrombus formation and reduce the risk of thromboembolisation on one hand and prolong the endosaccular clot formation on the other. Due to the prolonged treatment procedure, further wall inflammation and damage may occur due to the presence of an incomplete clot partially covering the aneurysm wall, increasing the risk of post-treatment rupture [21, 181]. Moreover, the increased time of clotting due to the prescription of antiplatelets and anticoagulants can further increase the risk of bleeding in patients with endovascular treatments [180].

Mechanisms of intra-aneurysmal thrombosis

It has been shown that adverse haemodynamic stresses on the aneurysm wall can result in wall inflammation and damage to the intact arterial endothelium [20]. The cell-based model of coagulation [182] provides an explanation for spontaneous thrombosis resulting from the endothelial damage and exposure of vascular tissue factor (TF) to the circulating blood in the aneurysm sac. WSS at regions where flow is low and multidirectional or at regions where flow variations are dominated by frequencies higher than the systemic flow frequency (the heart rate) have been shown to correlate with the pro-inflammatory response of the endothelial cells [115, 183]. Inflamed endothelium expresses the NF-κB transcription factor (a nuclear transcription factor that can be activated by environmental signals, like WSS, and mediate wall inflammation and weakening), leading to upregulation of blood borne TF, which can subsequently trigger spontaneous thrombosis in such regions [184, 185]. Platelet activation and aggregation within the recirculation regions followed by deposition in regions of low flow has also been used to explain spontaneous coagulation in aneurysms [186, 187].

As far as device-induced coagulation in aneurysms is considered, pro-coagulant alterations in aneurysm haemodynamics, platelet activation as a result of blood contact with the deployed devices, and shear-induced platelet activation are key factors in initiating endosaccular thrombosis.

Intra-aneurysmal flow reduction using endovascular devices is thought to create dead zones where the flow stasis favours platelet adhesion and activation, a key step in the thrombosis process [22, 23]. Such flow stasis can also damage the endothelium and expose sub-endothelial TF [188]. Blood contact with the artificial material (the deployed devices) is hypothesised to also be responsible for the initiation of blood coagulation inside the aneurysm sac [189, 190]. Xiang et al. [22] showed that platelets can become activated in high-shear regions near the flow diverter stent struts and can be transferred to and deposited in low-flow regions in the sac. They further distinguished between white and red thrombi, where the former favours aneurysm healing and the latter leads to further wall weakening and the ultimate aneurysm rupture after flow diverter placement.

Computational models for spontaneous thrombosis in aneurysms

The most challenging part of a mechanistic model of thrombus formation in aneurysms is the mechanism used to describe thrombosis initiation. It has been observed that blood clots form or at least deposit in the regions where blood flow is extremely low and multidirectional [25, 191-193]. However, it is not yet well understood whether clotting starts extrinsically due to the endothelial damage and TF exposure in disturbed flow regions, i.e., aneurysmal wall regions where haemodynamic stresses are extremely low and multidirectional; or, intrinsically due to platelet activation and aggregation and exposure of blood borne TF under certain haemodynamic conditions [194]. Coagulation models in aneurysms can be classified into two main groups. The former only characterise blood flow in aneurysms and do not include any biochemical reactions. The latter, however, couple both flow and reaction to model coagulation in aneurysms. Some models include additional parts that consider the mechanical interactions between the clot and the blood flow field.

Rayz et al. [25, 195] and Ouared et al. [24, 196] correlated flow velocity, flow residence time (RT) and WSS with clot formation and simulated clotting in aneurysms without considering the biochemical reactions. For three patients with magnetic resonance imaging (MRI) scans before and after thrombus formation, Rayz et al. [195] showed that blood clots developed in regions with low WSS and high RT. They revealed a correlation between the location of intraluminal blood clots and regions of high RT and low WSS. Zimny et al. [197] classified thrombosis initiation mechanisms in aneurysms into intrinsic and extrinsic mechanisms. In their multiscale model, intrinsic mechanisms initiated clotting through platelet activation by the inflamed wall or by the contact of blood with external devices (e.g., coils and stents) and extrinsic mechanisms initiate clotting through exposure of TF due to damage to the aneurysm wall. Such damage was considered to be a result of post-treatment flow alterations in the sac or any cuts that occurred during the deployment procedure. They finally extended the mesoscale model presented by Ouared et al. [24, 196] to a three-dimensional aneurysm model and simulated flow-mediated thrombus generation based on a threshold on aneurysmal WSS under which thrombosis initiates. De Sousa et al. [23] simulated flow in ten patient-specific aneurysms and showed that spontaneous thrombosis was present in aneurysms with low shear rate and suppressed pulsatility. They also showed for three aneurysms treated with flow diverters that after flow diverter deployment, the aneurysmal shear rate fell below a certain threshold that has been correlated with the onset of thrombosis generation.

Although such models can provide some information about the possibility of presence of endosaccular thrombosis under certain aneurysmal morphology or haemodynamic environment, they will not provide enough information about the morphology of the aneurysmal blood clot and its interaction with the aneurysmal blood flow. Since these models do not include the underlying biochemical reactions, they cannot be used to predict effects of the chemical composition of blood or use of anticoagulants on spontaneous clotting or the final outcome of endovascular treatment. Coupling blood flow with a network of biochemical reactions, Bedekar et al. [26] and Biasetti et al. [198]

simulated clot formation in intracranial and abdominal aortic aneurysms, respectively. They both used TF exposure on the aneurysm wall as the initiator of the clotting process and assigned a prescribed concentration of TF on the aneurysm wall as boundary condition. This approach benefited from a biochemical web of surface reactions to model clot formation on the aneurysm wall; however, it assumed that TF was uniformly exposed on the aneurysm wall and initiated the coagulation cascade. On the contrary, it has been observed that inflammatory lesions and endothelial damage, which are thought to be responsible for TF exposure, are localised phenomena resulted from region-specific adverse haemodynamic conditions. Malaspinas et al. [192] set up a series of in vitro experiments and obtained WSS thresholds below which coagulation starts in idealised aneurysm geometries. Then, they used those thresholds to simulate clotting in two real aneurysms and successfully validated their results against patient-specific medical images. Although Malaspinas et al. [192] took a threshold-based approach to study spontaneous clotting in aneurysms, they simulated the underlying biochemical reactions; that is, the threshold has been used as the initiator of a web of chemical reactions. This makes their model capable of investigating the effect of patient-specific deficiencies in certain coagulation factors and/or the effect of anticoagulants on the clotting time and the final percentage of aneurysm occlusion.

Computational models for device-induced thrombosis in aneurysms

Xiang et al. [22] presented a model of blood flow in stented aneurysms, and demonstrated that blood flow near stent struts can provide shear rates high enough to activate platelets and trigger blood coagulation in the aneurysm sac where the flow is low enough for platelets to aggregate. Ngoepe et al. [199] coupled flow and biochemistry to simulate both spontaneous and stent-induced thrombosis in patient-specific aneurysm geometries. They used a level-set method to track the clot surface at each instance of the time and consider the effect of clot on the flow domain. They considered vascular TF as the sole initiator of the clotting process; however, instead of a uniform exposure of TF on the aneurysm wall, they used a shear rate threshold below which TF can be expressed on the wall and initiate the clotting process. This allowed coagulation to start only on the portions of the endothelium that are expected to be damaged, which is more physiologically relevant than exposing TF uniformly on the aneurysm lumen.

Recently, observing the fact blood clotting in aneurysms is not necessarily triggered by the exposure of extravascular TF due to the wall damage, Ou et al. [193] presented a model with more emphasis on the blood-borne TF as the initiator of stasis-induced thrombosis in aneurysms. To concentrate on the role played by the blood-borne TF, they ignored exposure of TF on the sub-endothelium and thrombogenicity of the flow-diverter. They hypothesised that accumulation of blood-borne TF in aneurysmal dead zones, where flow is low enough, is responsible for the initiation of thrombosis in those regions. The validity of their proposed model was supported by in vivo observations of surgically induced stasis in ligated right common carotid arteries of rats.

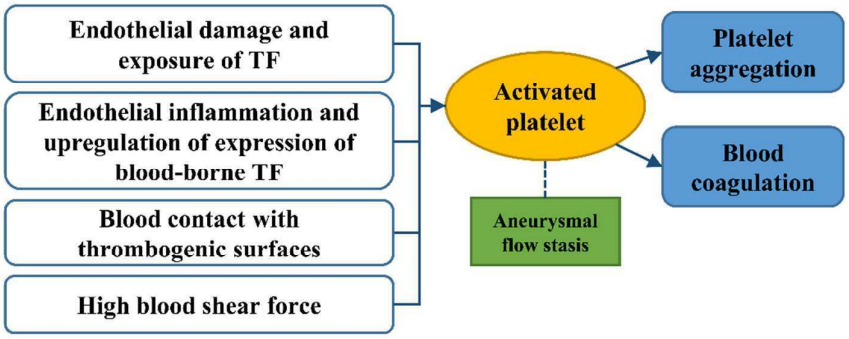

Figure 6. Possible mechanisms of intra-aneurysmal thrombosis

Uncertainty in computational models of blood coagulation

Blood coagulation, either as part of haemostatic system or under pathological conditions, is a very complex system with several sources of uncertainty. One may consider the lack of in vivo experimental data and the limited knowledge on the underlying pro- and anticoagulant mechanisms as the main sources of uncertainty in such a complex process. It has been implied that neither cascade nor cell-based models of coagulation can satisfactorily explain in vivo coagulation in pathologies like intracranial aneurysms [189]. The role of the vessel wall in chemical initiation and hosting the coagulation process and interactive effects of the clot and blood flow field are still uncertain [26, 199, 200].

According to Virchow's triad, thrombosis can be initiated as a result of damage to the endothelium, damage to the blood itself, or under certain blood flow conditions. Particularly, as depicted in Figure 6, coagulation in aneurysms can be initiated due to 1) platelet activation as a result of endothelial damage and contact of blood with the vascular TF, 2) platelet activation as a response to upregulation of the blood-borne TF due to pro-inflammatory response of the endothelium, 3) platelet activation as a result of blood contact with thrombogenic surface of endovascular implants, and 4) platelet activation as a response to high blood shear force at high shear regions like near the flow-diverter struts. Blood stasis (dead zones) in complex aneurysmal geometries is always a favourable region for activated platelets to deposit and trigger blood coagulation. When considering blood coagulation in a given aneurysm, it is unclear beforehand if any or all of the above mentioned mechanisms are responsible for initiation or amplification of the thrombosis. Moreover, none of the current models developed to simulate blood coagulation in aneurysms include all of the above mechanisms or measure the relative importance of them for a particular aneurysm.

Insufficient experimental data and uncertain role of the coagulation factors can even increase the level of uncertainty of the current models. For example, activation of the coagulation factor XII (a coagulation plasma protein that can be activated on artificial surfaces) in the presence of endovascular implants, which plays an important role in amplification of the coagulation, is not included in the cell-based model of coagulation [189].

Intra-subject variability in blood composition and pathologic deficiencies of certain coagulation factors can also increase the amount of uncertainty in coagulation modelling. It has been shown that uncertainty in the concentration of certain coagulation factors can result in completely different thrombin generation curves in a single patient. This can even be generalised to inter-subject, age-, sex-, and lifestyle-related variabilities in concentration of coagulation factors. These variabilities can also affect kinetics of the underlying reactions in terms of their rate constants. Danforth et al. [201] and Luan et al. [202, 203] investigated uncertainties in the reaction rate constants and showed that the

predictive capability of the entire model is highly sensitive to variabilities in some of the numerous rate constants involved in a biochemical model of coagulation.

Conclusions

Endovascular treatment of intracranial aneurysms requires evaluating the best treatment options in terms of efficacy and safety. Whether a certain endovascular treatment leads to formation of a stable clot in a specific aneurysm is a question that challenges neurointerventionalists. Endovascular planning systems that would allow pre-interventional assessment of aneurysmal haemodynamics before and after virtual treatment are potentially valuable clinical tools. Underpinning such systems, computational fluid dynamics (CFD) alongside other computational techniques for creating image-based vascular surface models and models of endovascular devices have already been extensively used to characterise intra-aneurysmal blood flow, and to understand the interplay between blood flow, aneurysm rupture risk, and endovascular treatment outcome. This paper overviewed the state-of-the-art in this area; and highlighted the importance of future efforts concentrating in device-induced thrombosis and uncertainty modelling in the context of VETMs.

We have presented a review of the current status of vascular anatomy and blood flow models, endovascular device deployment models, and blood coagulation models as the main ingredients that can be integrated into a VETM to help clinicians in the management of intracranial aneurysms. To provide a complete picture of treatment outcome, current systems for VETM need to be extended to incorporate post-treatment aneurysmal response and account, for instance, for the mechanisms of clot formation in the presence of endovascular devices. Although efforts exist to model intra-aneurysmal blood coagulation [200, 204], none of the current models include all of the underlying mechanisms of intra-aneurysmal coagulation (see Figure 6) or measure the relative importance of them for a particular aneurysm. Most of the models have not been personalised or are difficult to personalise based on available patient-specific data. Stratification [205, 206] and success criteria for endovascular treatment need to be established that objectively define the ideal outcome in a way that could be used by the modelling community as part of a treatment optimisation framework. Therefore, future research will have to first bridge the gap between available empirical evidence from clinical studies as to what constitutes and leads to a successful treatment outcome and the technical ability to computationally model the complex interplay between factors due to the anatomy, haemodynamics, blood clot, and endovascular device. This underlying complexity, on the other hand, will have to be modelled in a judiciously simplified manner not only to make the problem computationally tractable while remaining faithful to key mechanisms but also to enable personalisation of model parameters to limited patient-specific data. At the same time, current attempts to create advanced haemodynamic surrogates for intra-aneurysmal biological phenotypes (e.g. thrombosis) [23, 25, 195, 207], should be further validated against in vivo observations and potentially used to develop more accurate predictors of intra-aneurysmal thrombosis that those attainable by simulating even simplified models the underlying complex biological mechanisms.

In an editorial, Kallmes [28] expressed concerns regarding the status of computational studies on intracranial aneurysms and their clinical relevance. Two challenges were raised: 1) Can the virtual endovascular treatment model (VETM) be used to predict flow quantities that are useful in clinical diagnosis and prognosis? 2) Do the numerous modelling assumptions and related uncertainties make the results questionable? In another editorial, Cebral and Meng [208] emphasised that certain approximations and simplifications are needed in CFD studies to make them more cost effective and feasible. They suggested that what is important is measuring the effect of those assumptions on model outcomes and their relative importance, which could be evaluated using sensitivity analysis techniques. In this work, we have reviewed the three main ingredients of an image-based patient-specific virtual endovascular treatment model for intracranial aneurysms. Each of these sub-models

is prone to uncertainties, which should be addressed in order to make the virtual endovascular treatment model reliable as well as patient-specific. For those uncertainties that we found enough quantitative analyses, we performed a meta-analysis to identify their pooled effect. As presented in Table 1, we categorised uncertainties into: 1) those for which a meta-analysis has been performed and thus their effects are supported by the highest level of evidence, 2) those which have been studied in the literature but for which we could not perform a meta-analyses due to effects not being reported quantitatively or having only been considered in a limited number of studies, and 3) those which have not been studied yet in the context of IAs and thus their effect on the model outcomes is not still clear.

Virtual endovascular treatment models are influenced by several sources of uncertainty that need to be accounted for when interpreting the results of their predictions. Uncertainty handling is relevant to most computational biomechanics problems but can become particularly severe in complex multi-scale models. Meta-analyses have been performed on three well-known sources of uncertainty, and the uncertainties arising from *vascular wall distensibility* and *inflow waveform variabilities* showed effect sizes (Hedge's g) of 0.34, 95% CI [0.22, 0.45], p-value < 0.001, and 0.3, 95% CI [0.08,0.52], p-value = 0.003, respectively. Significance of non-rigid FSI models in future understanding of complex biomechanical processes at the aneurysm wall has also been pointed out by Chung and Cebral [103]. Physiologically realistic FSI models of aneurysms require measuring local variations of wall mechanical properties over highly heterogeneous pathologic aneurysms' wall which is not easily achievable in routine clinical practice. In future, such uncertainties should be addressed by 1) using more accurate techniques for measuring model input parameters (*uncertainty mitigation*), 2) consideration to the propagation of uncertainties from input parameters into the model outputs by reporting confidence intervals and sensitivities instead of deterministic results (*uncertainty exploration*), or 3) replacing model outputs with other alternative variables, which carry the same information but are less sensitive to the unknown model parameters (*sensitivity reduction*). Specifically, more advanced imaging techniques can provide higher quality images of the vascular lumen along with fully automatic segmentation techniques that do not require *a posteriori* manual editing and can eliminate some of the geometric uncertainty. Conducting more experimental studies regarding the mechanisms underlying thrombosis, particularly in aneurysms, can reduce model uncertainties in aneurysmal clotting and thus produce more reliable virtual treatment outcome predictions. However, inherent uncertainties in the systemic flow (and several other model parameters) cannot be eliminated. In such cases, advanced uncertainty quantification techniques [111, 209, 210] can be used to systematically explore the effects of these uncertainties. The concept of *personalisation* should not be limited to deterministic identification of model parameters at a particular moment in time. Instead, model parameters should be treated as uncertain and/or fluctuating quantities; and uncertainty quantification techniques should be employed to propagate those uncertainties through the virtual treatment models in order to produce confidence intervals and sensitivities associated with the model predictions.

Table 1. Major sources of uncertainty in different sub-models of a typical endovascular treatment model.

a) Uncertainties for which a meta-analysis has been performed

Source of Uncertainty	Reference(s) First Author (Year)	Summary Effect (Hedges' *g*) Mean (95% CI)
Wall distensibility	Torii et al. (2009) Bazilevs et al. (2010a) Bazilevs et al. (2010b) Takizawa et al. (2012)	0.34 (0.22 – 0.45)
Inlet flow rate waveform (inter-subject variability)	Karmonik et al. (2010) McGah et al. (2013) Jansen et al. (2014)	0.30 (0.08 – 0.52)
Blood rheology	Fisher & Rossmann (2009) Morales et al. (2013) Castro et al. (2014)	0.02 (-0.04 – 0.07)

b) Uncertainties for which a meta-analysis has not been performed

Source of Uncertainty	Reference(s) First Author (Year)	Main Findings
Segmentation and reconstruction accuracy	Cebral (2005) Castro (2006)	Overestimation of neck size by CTA compared to 3DRA lead to a 44.2% difference in time-and-space-averaged WSS over the aneurysm sac [39].
	Gambaruto (2011) Geers (2011)	Overestimation of neck size by 3DRA compared to 2D DSA lead to differences up to 98% in maximal WSS over the aneurysm sac [211].
	Mikhal (2013)	Reconstruction smoothing level can affect aneurysmal WSS by 15% [44].
	Schneiders (2013)	Reconstruction of aneurysm and parent vessel surface models significantly affect aneurysmal haemodynamics. Special care should be taken about removing kissing vessels, overestimation of aneurysm neck size by CTA and 3DRA, smoothing levels, and parent vessel reconstruction.
Length of parent vessel proximal to the aneurysm	Pereira (2013) Hodis (2015) Valen-Sendstad (2015)	Length of proximal parent vessel have a large effect on the aneurysmal haemodynamics (approximately 20% on the aneurysmal WSS [95]). Parent vessels should at least be truncated as far upstream as images allow, preferably below the cavernous segment on ICA.
Outlet boundary conditions	Ramalho (2012)	Outflow boundary conditions highly influence the aneurysmal haemodynamics (approximately 20% on the aneurysmal WSS) when multiple outlets are present. 0D and 1D outlet boundary conditions provide realistic flow split between branches when tuned carefully.
Moving parent arteries	Sforza (2010)	Pulsating intracranial vasculature motion has small effects on the aneurysmal haemodynamics (less than 5% on the aneurysmal WSS).
Using different CFD solvers	Steinman (2012)	Standard deviations of below 9% for cycle-averaged and peak systolic velocity and pressure.

Discretisation schemes	Valen-Sendstad (2014)	Strong correlation (R^2 > 0.9) between time-averaged WSS magnitudes between values obtained from normal and high resolution simulations. Weak correlation (R^2 = 0.23) between OSI values predicted by normal and high resolution simulations.
Endovascular device deployment model structure (imprecise governing equations)	Morales (2012)	Modelling aneurysmal coils explicitly or approximating them by a porous medium will highly affect the predictions of post-treatment haemodynamics (approximately 70% difference in the post-treatment intra-aneurysmal velocity).
	Levitt (2016)	Differences up to 50% and 130%, respectively in post-treatment time-averaged WSS and OSI values averaged over the aneurysm sacs obtained from explicit and porous medium models of coiled
	Raschi (2014)	Aneurysm-averaged WSS Differences of 10-25% between aneurysmal post-treatment haemodynamics predicted by explicit and porous medium models of the deployed stents.
	Augsburger (2010)	Relative root mean square errors of 21%-24% in mean WSS magnitude averaged over the entire sac and 45%-81% in mean WSS magnitude averaged over the aneurysm dome between simulations with flow diverters modelled either as porous medium or explicitly.
Intra-procedural systemic flow alterations	Mut (2014)	Intra-procedural parent vessel flow rate alterations greater than 30% can result can result in a 30-80% change in the aneurysmal haemodynamic variables.

c) Uncertainties that have so far not been studied in intracranial aneurysm simulations

Source of Uncertainty
Intra-procedural alterations in parent vessel geometry
Blood coagulation model structure (missing reactions etc.)
Parameters of mechanistic models of medical devices (coils and stents)
Variabilities in blood composition and coagulation kinetic reaction rates in normal or pathological conditions

References

1. Rinkel GJ, Djibuti M, Algra A, Van Gijn J. Prevalence and risk of rupture of intracranial aneurysms a systematic review. *Stroke* 1998, 29:251-256.
2. Krings T, Mandell DM, Kiehl T-R, Geibprasert S, Tymianski M, Alvarez H, Hans F-J. Intracranial aneurysms: from vessel wall pathology to therapeutic approach. *Nat Rev Neurol* 2011, 7:547-559.
3. Gabriel RA, Kim H, Sidney S, McCulloch CE, Singh V, Johnston SC, Ko NU, Achrol AS, Zaroff JG, Young WL. Ten-year detection rate of brain arteriovenous malformations in a large, multiethnic, defined population. *Stroke* 2010, 41:21-26.
4. Bederson JB, Awad IA, Wiebers DO, Piepgras D, Haley EC, Brott T, Hademenos G, Chyatte D, Rosenwasser R, Caroselli C. Recommendations for the management of patients with unruptured intracranial aneurysms: a statement for healthcare professionals from the stroke council of the American Heart Association. *Circulation* 2000, 102:2300-2308.
5. Steiner T, Juvela S, Unterberg A, Jung C, Forsting M, Rinkel G. European Stroke Organization guidelines for the management of intracranial aneurysms and subarachnoid haemorrhage. *Cerebrovasc Dis* 2013, 35:93-112.
6. Chang H-H, Duckwiler GR, Valentino DJ, Chu WC. Computer-assisted extraction of intracranial aneurysms on 3D rotational angiograms for computational fluid dynamics modeling. *Med Phys* 2009, 36:5612-5621.
7. Firouzian A, Manniesing R, Flach ZH, Risselada R, van Kooten F, Sturkenboom MC, van der Lugt A, Niessen WJ. Intracranial aneurysm segmentation in 3D CT angiography: Method and quantitative validation with and without prior noise filtering. *Eur J Radiol* 2011, 79:299-304.
8. Hernandez M, Frangi AF. Non-parametric geodesic active regions: method and evaluation for cerebral aneurysms segmentation in 3DRA and CTA. *Med Image Anal* 2007, 11:224-241.
9. Bouillot P, Brina O, Ouared R, Yilmaz H, Farhat M, Erceg G, Lovblad K-O, Vargas MI, Kulcsar Z, Pereira VM. Geometrical deployment for braided stent. *Med Image Anal* 2016, 30:85-94.
10. Larrabide I, Kim M, Augsburger L, Villa-Uriol MC, Rüfenacht D, Frangi AF. Fast virtual deployment of self-expandable stents: method and in vitro evaluation for intracranial aneurysmal stenting. *Med Image Anal* 2012, 16:721-730.
11. Ma D, Dargush GF, Natarajan SK, Levy EI, Siddiqui AH, Meng H. Computer modeling of deployment and mechanical expansion of neurovascular flow diverter in patient-specific intracranial aneurysms. *J Biomech* 2012, 45:2256-2263.
12. Morales HG, Larrabide I, Aguilar ML, Geers AJ, Macho JM, San Roman L, Frangi AF. Comparison of two techniques of endovascular coil modeling in cerebral aneurysms using CFD. In: *ISBI*: IEEE; 2012, 1216-1219.
13. Cebral JR, Castro MA, Appanaboyina S, Putman CM, Millan D, Frangi AF. Efficient pipeline for image-based patient-specific analysis of cerebral aneurysm hemodynamics: technique and sensitivity. *IEEE Trans Med Imaging* 2005, 24:457-467.
14. Villa-Uriol M, Larrabide I, Pozo J, Kim M, De Craene M, Camara O, Zhang C, Geers A, Bogunović H, Morales H. Cerebral aneurysms: a patient-specific and image-based management pipeline. In: *Computational Vision and Medical Image Processing*: Springer; 2011, 327-349.
15. Villa-Uriol M-C, Larrabide I, Pozo J, Kim M, Camara O, De Craene M, Zhang C, Geers A, Morales H, Bogunović H. Toward integrated management of cerebral aneurysms. *Philos T Roy Soc A* 2010, 368:2961-2982.
16. Walcott BP, Reinshagen C, Stapleton CJ, Choudhri O, Rayz V, Saloner D, Lawton MT. Predictive modeling and in vivo assessment of cerebral blood flow in the management of complex cerebral aneurysms. *J Cereb Blood Flow Metab* 2016, 36:998-1003.
17. Bhogal P, Pérez MA, Ganslandt O, Bäzner H, Henkes H, Fischer S. Treatment of posterior circulation non-saccular aneurysms with flow diverters: a single-center experience and

review of 56 patients. *J Neurointerv Surg* 2016:Published Online First: 11 November 2016, doi: 2010.1136/neurintsurg-2016-012781.

18. Shapiro M, Becske T, Riina HA, Raz E, Zumofen D, Nelson PK. Non-saccular vertebrobasilar aneurysms and dolichoectasia: a systematic literature review. *J Neurointerv Surg* 2014, 6:389-393.
19. Iosif C, Ponsonnard S, Roussie A, Saleme S, Carles P, Ponomarjova S, Pedrolo-Silveira E, Mendes G, Waihrich E, Couquet C. Jailed Artery Ostia Modifications After Flow-Diverting Stent Deployment at Arterial Bifurcations: A Scanning Electron Microscopy Translational Study. *Neurosurgery* 2016, 79:473-480.
20. Meng H, Tutino V, Xiang J, Siddiqui A. High WSS or low WSS? Complex interactions of hemodynamics with intracranial aneurysm initiation, growth, and rupture: toward a unifying hypothesis. *Am J Neuroradiol* 2014, 35:1254-1262.
21. Kulcsár Z, Houdart E, Bonafe A, Parker G, Millar J, Goddard A, Renowden S, Gál G, Turowski B, Mitchell K. Intra-aneurysmal thrombosis as a possible cause of delayed aneurysm rupture after flow-diversion treatment. *Am J Neuroradiol* 2011, 32:20-25.
22. Xiang J, Ma D, Snyder KV, Levy EI, Siddiqui AH, Meng H. Increasing flow diversion for cerebral aneurysm treatment using a single flow diverter. *Neurosurgery* 2014, 75:286-294.
23. de Sousa DR, Vallecilla C, Chodzynski K, Jerez RC, Malaspinas O, Eker OF, Ouared R, Vanhamme L, Legrand A, Chopard B. Determination of a shear rate threshold for thrombus formation in intracranial aneurysms. *J Neurointerv Surg* 2015:853-858.
24. Ouared R, Chopard B, Stahl B, Rüfenacht DA, Yilmaz H, Courbebaisse G. Thrombosis modeling in intracranial aneurysms: a lattice Boltzmann numerical algorithm. *Comput Phys Commun* 2008, 179:128-131.
25. Rayz V, Boussel L, Lawton M, Acevedo-Bolton G, Ge L, Young W, Higashida R, Saloner D. Numerical modeling of the flow in intracranial aneurysms: prediction of regions prone to thrombus formation. *Ann Biomed Eng* 2008, 36:1793-1804.
26. Bedekar A, Pant K, Ventikos Y, Sundaram S. A computational model combining vascular biology and haemodynamics for thrombosis prediction in anatomically accurate cerebral aneurysms. *Food Bioprod Process* 2005, 83:118-126.
27. Ngoepe M, Ventikos Y. Computational modelling of clot development in patient-specific cerebral aneurysm cases. *J Thromb Haemost* 2016, 14:262-272.
28. Kallmes DF. Point: CFD—computational fluid dynamics or confounding factor dissemination. *Am J Neuroradiol* 2012, 33:395-396.
29. Borenstein M, Hedges LV, Higgins J, Rothstein HR. *Introduction to meta-analysis*: Wiley Online Library; 2009.
30. Chappell ET, Moure FC, Good MC. Comparison of computed tomographic angiography with digital subtraction angiography in the diagnosis of cerebral aneurysms: a meta-analysis. *Neurosurgery* 2003, 52:624-631.
31. Sailer AM, Wagemans BA, Nelemans PJ, de Graaf R, van Zwam WH. Diagnosing intracranial aneurysms with MR angiography systematic review and meta-analysis. *Stroke* 2014, 45:119-126.
32. van Rooij WJ, Sprengers M, de Gast AN, Peluso J, Sluzewski M. 3D rotational angiography: the new gold standard in the detection of additional intracranial aneurysms. *Am J Neuroradiol* 2008, 29:976-979.
33. Piotin M, Gailloud P, Bidaut L, Mandai S, Muster M, Moret J, Rüfenacht D. CT angiography, MR angiography and rotational digital subtraction angiography for volumetric assessment of intracranial aneurysms. An experimental study. *Neuroradiology* 2003, 45:404-409.
34. Ramachandran M, Retarekar R, Harbaugh RE, Hasan D, Policeni B, Rosenwasser R, Ogilvy C, Raghavan ML. Sensitivity of quantified intracranial aneurysm geometry to imaging modality. *Cardiovasc Eng Technol* 2013, 4:75-86.

35. Anxionnat R, Bracard S, Ducrocq X, Trousset Y, Launay L, Kerrien E, Braun M, Vaillant R, Scomazzoni F, Lebedinsky A. Intracranial aneurysms: clinical value of 3D digital subtraction angiography in the therapeutic decision and endovascular treatment *Radiology* 2001, 218:799-808.
36. Missler U, Hundt C, Wiesmann M, Mayer T, Brückmann H. Three-dimensional reconstructed rotational digital subtraction angiography in planning treatment of intracranial aneurysms. *Eur Radiol* 2000, 10:564-568.
37. Tanoue S, Kiyosue H, Kenai H, Nakamura T, Yamashita M, Mori H. Three-dimensional reconstructed images after rotational angiography in the evaluation of intracranial aneurysms: surgical correlation. *Neurosurgery* 2000, 47:866-871.
38. Castro MA, Putman CM, Cebral JR. Patient-specific computational modeling of cerebral aneurysms with multiple avenues of flow from 3D rotational angiography images. *Acad Radiol* 2006, 13:811-821.
39. Geers A, Larrabide I, Radaelli AG, Bogunovic H, Kim M, van Andel HG, Majoie C, VanBavel E, Frangi A. Patient-specific computational hemodynamics of intracranial aneurysms from 3D rotational angiography and CT angiography: an in vivo reproducibility study. *Am J Neuroradiol* 2011, 32:581-586.
40. Bogunović H, Pozo JM, Villa-Uriol MC, Majoie CB, van den Berg R, van Andel HAG, Macho JM, Blasco J, San Román L, Frangi AF. Automated segmentation of cerebral vasculature with aneurysms in 3DRA and TOF-MRA using geodesic active regions: an evaluation study. *Med Phys* 2011, 38:210-222.
41. Steinman DA, Milner JS, Norley CJ, Lownie SP, Holdsworth DW. Image-based computational simulation of flow dynamics in a giant intracranial aneurysm. *Am J Neuroradiol* 2003, 24:559-566.
42. Sen Y, Qian Y, Zhang Y, Morgan M. A comparison of medical image segmentation methods for cerebral aneurysm computational hemodynamics. In: *BMEI*: IEEE; 2011, 901-904.
43. Castro M, Putman C, Cebral J. Computational fluid dynamics modeling of intracranial aneurysms: effects of parent artery segmentation on intra-aneurysmal hemodynamics. *Am J Neuroradiol* 2006, 27:1703-1709.
44. Gambaruto AM, Janela J, Moura A, Sequeira A. Sensitivity of hemodynamics in a patient specific cerebral aneurysm to vascular geometry and blood rheology. *Math Biosci Eng* 2011, 8:409-423.
45. Geers AJ, Larrabide I, Radaelli A, Bogunovic H, Van Andel H, Majoie C, Frangi AF. Reproducibility of image-based computational hemodynamics in intracranial aneurysms: comparison of CTA and 3DRA. In: *ISBI*: IEEE; 2009, 610-613.
46. Spiegel M, Redel T, Zhang Y, Struffert T, Hornegger J, Grossman RG, Doerfler A, Karmonik C. Tetrahedral and polyhedral mesh evaluation for cerebral hemodynamic simulation–a comparison. In: *Conf Proc IEEE Eng Med Biol Soc*: IEEE; 2009, 2787-2790.
47. Taylor CA, Steinman DA. Image-based modeling of blood flow and vessel wall dynamics: applications, methods and future directions. *Ann Biomed Eng* 2010, 38:1188-1203.
48. Janiga G, Berg P, Beuing O, Neugebauer M, Gasteiger R, Preim B, Rose G, Skalej M, Thévenin D. Recommendations for accurate numerical blood flow simulations of stented intracranial aneurysms. *Biomed Tech (Berl)* 2013, 58:303-314.
49. Hodis S, Uthamaraj S, Smith AL, Dennis KD, Kallmes DF, Dragomir-Daescu D. Grid convergence errors in hemodynamic solution of patient-specific cerebral aneurysms. *J Biomech* 2012, 45:2907-2913.
50. Stuhne GR, Steinman DA. Finite-element modeling of the hemodynamics of stented aneurysms. *J Biomech Eng* 2004, 126:382-387.
51. Larrabide I, Geers AJ, Morales HG, Bijlenga P, Rüfenacht DA. Change in aneurysmal flow pulsatility after flow diverter treatment. *Comput Med Imag Grap* 2016, 50:2-8.

52. Janiga G, Rössl C, Skalej M, Thévenin D. Realistic virtual intracranial stenting and computational fluid dynamics for treatment analysis. *J Biomech* 2013, 46:7-12.
53. Löhner R. *Applied computational fluid dynamics techniques: an introduction based on finite element methods*: John Wiley & Sons; 2008.
54. Cebral JR, Lohner R. Efficient simulation of blood flow past complex endovascular devices using an adaptive embedding technique. *IEEE Trans Med Imaging* 2005, 24:468-476.
55. Appanaboyina S, Mut F, Löhner R, Putman C, Cebral J. Computational fluid dynamics of stented intracranial aneurysms using adaptive embedded unstructured grids. *Int J Numer Meth Fl* 2008, 57:475-493.
56. Ford MD, Alperin N, Lee SH, Holdsworth DW, Steinman DA. Characterization of volumetric flow rate waveforms in the normal internal carotid and vertebral arteries. *Physiol Meas* 2005, 26:477.
57. Gwilliam MN, Hoggard N, Capener D, Singh P, Marzo A, Verma PK, Wilkinson ID. MR derived volumetric flow rate waveforms at locations within the common carotid, internal carotid, and basilar arteries. *J Cereb Blood Flow Metab* 2009, 29:1975-1982.
58. Hoi Y, Wasserman BA, Xie YJ, Najjar SS, Ferruci L, Lakatta EG, Gerstenblith G, Steinman DA. Characterization of volumetric flow rate waveforms at the carotid bifurcations of older adults. *Physiol Meas* 2010, 31:291.
59. Nichols W, O'Rourke M, Vlachopoulos C. *McDonald's blood flow in arteries: theoretical, experimental and clinical principles*: CRC Press; 2011.
60. Shi Y, Lawford P, Hose R. Review of zero-D and 1-D models of blood flow in the cardiovascular system. *Biomed Eng Online* 2011, 10:33.
61. Grinberg L, Karniadakis GE. Outflow boundary conditions for arterial networks with multiple outlets. *Ann Biomed Eng* 2008, 36:1496-1514.
62. Olufsen MS, Nadim A, Lipsitz LA. Dynamics of cerebral blood flow regulation explained using a lumped parameter model. *Am J Physiol-Reg I* 2002, 282:R611-R622.
63. Formaggia L, Lamponi D, Quarteroni A. One-dimensional models for blood flow in arteries. *J Eng Math* 2003, 47:251-276.
64. Reymond P, Bohraus Y, Perren F, Lazeyras F, Stergiopulos N. Validation of a patient-specific one-dimensional model of the systemic arterial tree. *Am J Physiol-Heart C* 2011, 301:H1173-H1182.
65. Reymond P, Merenda F, Perren F, Rüfenacht D, Stergiopulos N. Validation of a one-dimensional model of the systemic arterial tree. *Am J Physiol-Heart C* 2009, 297:H208-H222.
66. Blanco P, Feijóo R, Urquiza S. A unified variational approach for coupling 3D–1D models and its blood flow applications. *Comput Method Appl M* 2007, 196:4391-4410.
67. Dempere-Marco L, Oubel E, Castro M, Putman C, Frangi A, Cebral J. CFD analysis incorporating the influence of wall motion: application to intracranial aneurysms. In: *Lect Notes Comput Sc*: Springer; 2006, 438-445.
68. Torii R, Oshima M, Kobayashi T, Takagi K, Tezduyar TE. Fluid–structure interaction modeling of aneurysmal conditions with high and normal blood pressures. *Comput Mech* 2006, 38:482-490.
69. Torii R, Oshima M, Kobayashi T, Takagi K, Tezduyar TE. Fluid–structure interaction modeling of a patient-specific cerebral aneurysm: influence of structural modeling. *Comput Mech* 2008, 43:151-159.
70. Radaelli A, Augsburger L, Cebral J, Ohta M, Rüfenacht D, Balossino R, Benndorf G, Hose D, Marzo A, Metcalfe R. Reproducibility of haemodynamical simulations in a subject-specific stented aneurysm model—a report on the Virtual Intracranial Stenting Challenge 2007. *J Biomech* 2008, 41:2069-2081.
71. Steinman DA, Hoi Y, Fahy P, Morris L, Walsh MT, Aristokleous N, Anayiotos AS, Papaharilaou Y, Arzani A, Shadden SC. Variability of computational fluid dynamics solutions for pressure

and flow in a giant aneurysm: the ASME 2012 Summer Bioengineering Conference CFD Challenge. *J Biomech Eng* 2013, 135:021016.

72. Martin DG, Ferguson EW, Wigutoff S, Gawne T, Schoomaker EB. Blood viscosity responses to maximal exercise in endurance-trained and sedentary female subjects. *J Appl Physiol* 1985, 59:348-353.
73. Kool MJ, Hoeks AP, Boudier HAS, Reneman RS, Van Bortel LM. Short and long-term effects of smoking on arterial wall properties in habitual smokers. *J Am Coll Cardiol* 1993, 22:1881-1886.
74. Bernsdorf J, Wang D. Non-Newtonian blood flow simulation in cerebral aneurysms. *Comput Math Appl* 2009, 58:1024-1029.
75. Valencia A, Zarate A, Galvez M, Badilla L. Non-Newtonian blood flow dynamics in a right internal carotid artery with a saccular aneurysm. *Int J Numer Meth Fl* 2006, 50:751-764.
76. Xiang J, Tremmel M, Kolega J, Levy EI, Natarajan SK, Meng H. Newtonian viscosity model could overestimate wall shear stress in intracranial aneurysm domes and underestimate rupture risk. *J Neurointerv Surg* 2011, 4:351-357.
77. Mazumdar J. *Biofluid mechanics*: World Scientific; 2015.
78. Castro MA, Olivares MCA, Putman CM, Cebral JR. Unsteady wall shear stress analysis from image-based computational fluid dynamic aneurysm models under Newtonian and Casson rheological models. *Med Biol Eng Comput* 2014, 52:827-839.
79. Fisher C, Rossmann JS. Effect of non-Newtonian behavior on hemodynamics of cerebral aneurysms. *J Biomech Eng* 2009, 131:091004.
80. Morales HG, Larrabide I, Geers AJ, Aguilar ML, Frangi AF. Newtonian and non-Newtonian blood flow in coiled cerebral aneurysms. *J Biomech* 2013, 46:2158-2164.
81. Huang C, Chai Z, Shi B. Non-newtonian effect on hemodynamic characteristics of blood flow in stented cerebral aneurysm. *Commun Comput Phys* 2013, 13:916-928.
82. Cavazzuti M, Atherton M, Collins M, Barozzi G. Beyond the virtual intracranial stenting challenge 2007: non-Newtonian and flow pulsatility effects. *J Biomech* 2010, 43:2645-2647.
83. Cavazzuti M, Atherton M, Collins M, Barozzi G. Non-Newtonian and flow pulsatility effects in simulation models of a stented intracranial aneurysm. *P I Mech Eng H* 2011, 225:597-609.
84. Morales HG, Bonnefous O. Unraveling the relationship between arterial flow and intra-aneurysmal hemodynamics. *J Biomech* 2015, 48:585-591.
85. Cohen J. A power primer. *Psychol Bull* 1992, 112:155-159.
86. Jansen I, Schneiders J, Potters W, van Ooij P, van den Berg R, van Bavel E, Marquering H, Majoie C. Generalized versus patient-specific inflow boundary conditions in computational fluid dynamics simulations of cerebral aneurysmal hemodynamics. *Am J Neuroradiol* 2014, 35:1543-1548.
87. Marzo A, Singh P, Larrabide I, Radaelli A, Coley S, Gwilliam M, Wilkinson ID, Lawford P, Reymond P, Patel U. Computational hemodynamics in cerebral aneurysms: the effects of modeled versus measured boundary conditions. *Ann Biomed Eng* 2011, 39:884-896.
88. McGah PM, Levitt MR, Barbour MC, Morton RP, Nerva JD, Mourad PD, Ghodke BV, Hallam DK, Sekhar LN, Kim LJ. Accuracy of computational cerebral aneurysm hemodynamics using patient-specific endovascular measurements. *Ann Biomed Eng* 2014, 42:503-514.
89. Karmonik C, Yen C, Diaz O, Klucznik R, Grossman RG, Benndorf G. Temporal variations of wall shear stress parameters in intracranial aneurysms—importance of patient-specific inflow waveforms for CFD calculations. *Acta Neurochir (Wien)* 2010, 152:1391-1398.
90. Bowker T, Watton P, Summers P, Byrne J, Ventikos Y. Rest versus exercise hemodynamics for middle cerebral artery aneurysms: a computational study. *Am J Neuroradiol* 2010, 31:317-323.
91. Geers A, Larrabide I, Morales H, Frangi A. Approximating hemodynamics of cerebral aneurysms with steady flow simulations. *J Biomech* 2014, 47:178-185.

92. Xiang J, Siddiqui A, Meng H. The effect of inlet waveforms on computational hemodynamics of patient-specific intracranial aneurysms. *J Biomech* 2014, 47:3882-3890.
93. Sarrami-Foroushani A, Lassila T, Gooya A, Geers AJ, Frangi AF. Uncertainty quantification of wall shear stress in intracranial aneurysms using a data-driven statistical model of systemic blood flow variability. *J Biomech* 2016, 49:3815–3823.
94. Valen-Sendstad K, Piccinelli M, KrishnankuttyRema R, Steinman DA. Estimation of inlet flow rates for image-based aneurysm CFD models: where and how to begin? *Ann Biomed Eng* 2015, 43:1422-1431.
95. Pereira V, Brina O, Gonzales AM, Narata A, Bijlenga P, Schaller K, Lovblad K, Ouared R. Evaluation of the influence of inlet boundary conditions on computational fluid dynamics for intracranial aneurysms: a virtual experiment. *J Biomech* 2013, 46:1531-1539.
96. Hodis S, Kargar S, Kallmes DF, Dragomir-Daescu D. Artery length sensitivity in patient-specific cerebral aneurysm simulations. *Am J Neuroradiol* 2015, 36:737-743.
97. Van Ooij P, Schneiders J, Marquering H, Majoie C, van Bavel E, Nederveen A. 3D cine phase-contrast MRI at 3T in intracranial aneurysms compared with patient-specific computational fluid dynamics. *Am J Neuroradiol* 2013, 34:1785-1791.
98. Humphrey J, Taylor C. Intracranial and abdominal aortic aneurysms: similarities, differences, and need for a new class of computational models. *Annu Rev Biomed Eng* 2008, 10:221.
99. Torii R, Oshima M, Kobayashi T, Takagi K, Tezduyar TE. Fluid–structure interaction modeling of blood flow and cerebral aneurysm: significance of artery and aneurysm shapes. *Comput Method Appl M* 2009, 198:3613-3621.
100. Takizawa K, Brummer T, Tezduyar TE, Chen PR. A comparative study based on patient-specific fluid-structure interaction modeling of cerebral aneurysms. *J Appl Mech* 2012, 79:010908.
101. Bazilevs Y, Hsu M-C, Zhang Y, Wang W, Kvamsdal T, Hentschel S, Isaksen J. Computational vascular fluid–structure interaction: methodology and application to cerebral aneurysms. *Biomech Model Mechan* 2010a, 9:481-498.
102. Bazilevs Y, Hsu M-C, Zhang Y, Wang W, Liang X, Kvamsdal T, Brekken R, Isaksen J. A fully-coupled fluid-structure interaction simulation of cerebral aneurysms. *Comput Mech* 2010b, 46:3-16.
103. Chung B, Cebral JR. CFD for evaluation and treatment planning of aneurysms: review of proposed clinical uses and their challenges. *Ann Biomed Eng* 2015, 43:122-138.
104. Torii R, Oshima M, Kobayashi T, Takagi K, Tezduyar TE. Influence of wall thickness on fluid–structure interaction computations of cerebral aneurysms. *Int J Numer Method Biomed Eng* 2010, 26:336-347.
105. Morales HG, Bonnefous O. Peak systolic or maximum intra-aneurysmal hemodynamic condition? Implications on normalized flow variables. *J Biomech* 2014, 47:2362-2370.
106. Mohamied Y, Rowland EM, Bailey EL, Sherwin SJ, Schwartz MA, Weinberg PD. Change of direction in the biomechanics of atherosclerosis. *Ann Biomed Eng* 2015, 43:16-25.
107. Wang C, Baker BM, Chen CS, Schwartz MA. Endothelial cell sensing of flow direction. *Arterioscler Thromb Vasc Biol* 2013, 33:2130-2136.
108. Ando J, Yamamoto K. Vascular mechanobiology endothelial cell responses to fluid shear stress. *Circ J* 2009, 73:1983-1992.
109. Wu M, KK, Thiagarajan M, P. Role of endothelium in thrombosis and hemostasis. *Annu Rev Med* 1996, 47:315-331.
110. Ramalho S, Moura A, Gambaruto A, Sequeira A. Sensitivity to outflow boundary conditions and level of geometry description for a cerebral aneurysm. *Int J Numer Method Biomed Eng* 2012, 28:697-713.

111. Schiavazzi D, Arbia G, Baker C, Hlavacek AM, Hsia T-Y, Marsden A, Vignon-Clementel I. Uncertainty quantification in virtual surgery hemodynamics predictions for single ventricle palliation. *Int J Numer Method Biomed Eng* 2015, 32:e02737.
112. Troianowski G, Taylor CA, Feinstein JA, Vignon-Clementel IE. Three-dimensional simulations in Glenn patients: clinically based boundary conditions, hemodynamic results and sensitivity to input data. *J Biomech Eng* 2011, 133:111006.
113. Janiga G, Berg P, Sugiyama S, Kono K, Steinman D. The Computational Fluid Dynamics Rupture Challenge 2013—Phase I: prediction of rupture status in intracranial aneurysms. *Am J Neuroradiol* 2015, 36:530-536.
114. Valen-Sendstad K, Steinman D. Mind the gap: impact of computational fluid dynamics solution strategy on prediction of intracranial aneurysm hemodynamics and rupture status indicators. *Am J Neuroradiol* 2014, 35:536-543.
115. Feaver RE, Gelfand BD, Blackman BR. Human haemodynamic frequency harmonics regulate the inflammatory phenotype of vascular endothelial cells. *Nat Commun* 2013, 4:1525.
116. Babiker MH, Chong B, Gonzalez LF, Cheema S, Frakes DH. Finite element modeling of embolic coil deployment: multifactor characterization of treatment effects on cerebral aneurysm hemodynamics. *J Biomech* 2013, 46:2809-2816.
117. Dequidt J, Duriez C, Cotin S, Kerrien E. Towards interactive planning of coil embolization in brain aneurysms. In: *Lect Notes Comput Sc*: Springer; 2009, 377-385.
118. Dequidt J, Marchal M, Duriez C, Kerien E, Cotin S. Interactive simulation of embolization coils: modeling and experimental validation. In: *Lect Notes Comput Sc*: Springer; 2008, 695-702.
119. Wei Y, Duriez C, Kerrien E, Allard J, Dequidt J, Cotin S. A (Near) real-time simulation method of aneurysm coil embolization. In: *Aneurysm*: InTech Open Access Publisher; 2012, 223-248.
120. Cha KS, Balaras E, Lieber BB, Sadasivan C, Wakhloo AK. Modeling the interaction of coils with the local blood flow after coil embolization of intracranial aneurysms. *J Biomech Eng* 2007, 129:873-879.
121. Groden C, Laudan J, Gatchell S, Zeumer H. Three-dimensional pulsatile flow simulation before and after endovascular coil embolization of a terminal cerebral aneurysm. *J Cereb Blood Flow Metab* 2001, 21:1464-1471.
122. Jou L-D, Saloner D, Higashida R. Determining intra-aneurysmal flow for coiled cerebral aneurysms with digital fluoroscopy. *Biomed Eng-App Bas C* 2004, 16:43-48.
123. Kakalis NM, Mitsos AP, Byrne JV, Ventikos Y. The haemodynamics of endovascular aneurysm treatment: a computational modelling approach for estimating the influence of multiple coil deployment. *IEEE Trans Med Imaging* 2008, 27:814-824.
124. Wei Y, Cotin S, Allard J, Fang L, Pan C, Ma S. Interactive blood-coil simulation in real-time during aneurysm embolization. *Comput Graph* 2011, 35:422-430.
125. Byun HS, Rhee K. CFD modeling of blood flow following coil embolization of aneurysms. *Med Eng Phys* 2004, 26:755-761.
126. Narracott A, Smith S, Lawford P, Liu H, Himeno R, Wilkinson I, Griffiths P, Hose R. Development and validation of models for the investigation of blood clotting in idealized stenoses and cerebral aneurysms. *J Artif Organs* 2005, 8:56-62.
127. Schirmer CM, Malek AM. Critical influence of framing coil orientation on intra-aneurysmal and neck region hemodynamics in a sidewall aneurysm model. *Neurosurgery* 2010, 67:1692-1702.
128. Bernardini A, Larrabide I, Petrini L, Pennati G, Flore E, Kim M, Frangi A. Deployment of self-expandable stents in aneurysmatic cerebral vessels: comparison of different computational approaches for interventional planning. *Comput Method Biomec* 2012, 15:303-311.

129. De Bock S, Iannaccone F, De Santis G, De Beule M, Mortier P, Verhegghe B, Segers P. Our capricious vessels: the influence of stent design and vessel geometry on the mechanics of intracranial aneurysm stent deployment. *J Biomech* 2012, 45:1353-1359.
130. Flore E, Larrabide I, Petrini L, Pennati G, Frangi A. Stent deployment in aneurysmatic cerebral vessels: assessment and quantification of the differences between Fast Virtual Stenting and Finite Element Analysis. In: *CI2BM09-MICCAI Workshop on Cardiovascular Interventional Imaging and Biophysical Modelling*: Springer-Verlag, Berlin, Germany; 2009, 790–797.
131. Kim JH, Kang TJ, Yu W-R. Mechanical modeling of self-expandable stent fabricated using braiding technology. *J Biomech* 2008, 41:3202-3212.
132. Augsburger L, Reymond P, Rufenacht D, Stergiopulos N. Intracranial stents being modeled as a porous medium: flow simulation in stented cerebral aneurysms. *Ann Biomed Eng* 2011, 39:850-863.
133. Morales HG, Bonnefous O. Modeling hemodynamics after flow diverter with a porous medium. In: *ISBI*: IEEE; 2014, 1324-1327.
134. Flórez-Valencia L, Orkisz M, Montagnat J. 3D graphical models for vascular-stent pose simulation. *Mach Grap Vision* 2004, 13:235-248.
135. Spranger K, Ventikos Y. Which spring is the best? Comparison of methods for virtual stenting. *IEEE Trans Biomed Eng* 2014, 61:1998-2010.
136. Jeong W, Han MH, Rhee K. Effects of framing coil shape, orientation, and thickness on intra-aneurysmal flow. *Med Biol Eng Comput* 2013, 51:981-990.
137. Aguilar ML, Morales HG, Larrabide I, Macho JM, San Roman L, Frangi AF. Effect of coil surface area on the hemodynamics of a patient-specific intracranial aneurysm: A computational study. In: *ISBI*: IEEE; 2012, 1180-1183.
138. Morales HG, Kim M, Vivas E, Villa-Uriol M-C, Larrabide I, Sola T, Guimaraens L, Frangi A. How do coil configuration and packing density influence intra-aneurysmal hemodynamics? *Am J Neuroradiol* 2011, 32:1935-1941.
139. Larrabide I, Aguilar M, Morales H, Geers A, Kulcsár Z, Rüfenacht D, Frangi A. Intra-aneurysmal pressure and flow changes induced by flow diverters: relation to aneurysm size and shape. *Am J Neuroradiol* 2013, 34:816-822.
140. Larrabide I, Geers AJ, Aguilar ML, Morales HG, Rufenacht D, Frangi AF. Influence of vascular morphology on hemodynamic changes after flow diverter placement in saccular intracranial aneurysms. *MICCAI-STENT* 2012:7-16.
141. Larrabide I, Geers AJ, Morales HG, Aguilar ML, Rüfenacht DA. Effect of aneurysm and ICA morphology on hemodynamics before and after flow diverter treatment. *J Neurointerv Surg* 2014, 7:272-280.
142. Wu Y-F, Yang P-F, Shen J, Huang Q-H, Zhang X, Qian Y, Liu J-M. A comparison of the hemodynamic effects of flow diverters on wide-necked and narrow-necked cerebral aneurysms. *J Clin Neurosci* 2012, 19:1520-1524.
143. Bouillot P, Brina O, Ouared R, Yilmaz H, Lovblad K-O, Farhat M, Pereira VM. Computational fluid dynamics with stents: quantitative comparison with particle image velocimetry for three commercial off the shelf intracranial stents. *J Neurointerv Surg* 2016, 8:309-315.
144. Kim M, Taulbee DB, Tremmel M, Meng H. Comparison of two stents in modifying cerebral aneurysm hemodynamics. *Ann Biomed Eng* 2008, 36:726-741.
145. Roszelle BN, Gonzalez LF, Babiker MH, Ryan J, Albuquerque FC, Frakes DH. Flow diverter effect on cerebral aneurysm hemodynamics: an in vitro comparison of telescoping stents and the Pipeline. *Neuroradiology* 2013, 55:751-758.
146. Tremmel M, Xiang J, Natarajan SK, Hopkins LN, Siddiqui AH, Levy EI, Meng H. Alteration of intraaneurysmal hemodynamics for flow diversion using Enterprise and Vision stents. *World Neurosurg* 2010, 74:306-315.

147. Babiker MH, Gonzalez LF, Ryan J, Albuquerque F, Collins D, Elvikis A, Frakes DH. Influence of stent configuration on cerebral aneurysm fluid dynamics. *J Biomech* 2012, 45:440-447.
148. Kim M, Larrabide I, Villa-Uriol M-C, Frangi AF. Hemodynamic alterations of a patient-specific intracranial aneurysm induced by virtual deployment of stents in various axial orientation. In: *ISBI*: IEEE; 2009, 1215-1218.
149. Kono K, Terada T. Hemodynamics of 8 different configurations of stenting for bifurcation aneurysms. *Am J Neuroradiol* 2013, 34:1980-1986.
150. Roszelle BN, Nair P, Gonzalez LF, Babiker MH, Ryan J, Frakes D. Comparison among different high porosity stent configurations: hemodynamic effects of treatment in a large cerebral aneurysm. *J Biomech Eng* 2014, 136:021013.
151. Augsburger L, Farhat M, Reymond P, Fonck E, Kulcsar Z, Stergiopulos N, Rüfenacht DA. Effect of flow diverter porosity on intraaneurysmal blood flow. *Clin Neuroradiol* 2009, 19:204-214.
152. Liou T-M, Li Y-C. Effects of stent porosity on hemodynamics in a sidewall aneurysm model. *J Biomech* 2008, 41:1174-1183.
153. Mut F, Cebral J. Effects of flow-diverting device oversizing on hemodynamics alteration in cerebral aneurysms. *Am J Neuroradiol* 2012, 33:2010-2016.
154. Ma D, Xiang J, Choi H, Dumont TM, Natarajan S, Siddiqui A, Meng H. Enhanced aneurysmal flow diversion using a dynamic push-pull technique: an experimental and modeling study. *Am J Neuroradiol* 2014, 35:1779-1785.
155. Janiga G, Daróczy L, Berg P, Thévenin D, Skalej M, Beuing O. An automatic CFD-based flow diverter optimization principle for patient-specific intracranial aneurysms. *J Biomech* 2015, 48:3846-3852.
156. Li C, Wang S, Chen J, Yu H, Zhang Y, Jiang F, Mu S, Li H, Yang X. Influence of hemodynamics on recanalization of totally occluded intracranial aneurysms: a patient-specific computational fluid dynamic simulation study: Laboratory investigation. *J Neurosurg* 2012, 117:276-283.
157. Luo B, Yang X, Wang S, Li H, Chen J, Yu H, Zhang Y, Zhang Y, Mu S, Liu Z. High shear stress and flow velocity in partially occluded aneurysms prone to recanalization. *Stroke* 2011, 42:745-753.
158. Graziano F, Russo V, Wang W, Khismatullin D, Ulm A. 3D computational fluid dynamics of a treated vertebrobasilar giant aneurysm: a multistage analysis. *Am J Neuroradiol* 2013, 34:1387-1394.
159. Park W, Song Y, Park KJ, Koo H-W, Yang K, Suh DC. Hemodynamic Characteristics Regarding Recanalization of Completely Coiled Aneurysms: Computational Fluid Dynamic Analysis Using Virtual Models Comparison. *Neurointervention* 2016, 11:30-36.
160. Chung B, Mut F, Kadirvel R, Lingineni R, Kallmes DF, Cebral JR. Hemodynamic analysis of fast and slow aneurysm occlusions by flow diversion in rabbits. *J Neurointerv Surg* 2015, 7:931-935.
161. Mut F, Raschi M, Scrivano E, Bleise C, Chudyk J, Ceratto R, Lylyk P, Cebral JR. Association between hemodynamic conditions and occlusion times after flow diversion in cerebral aneurysms. *J Neurointerv Surg* 2014, 7:286-290.
162. Kulcsár Z, Augsburger L, Reymond P, Pereira VM, Hirsch S, Mallik AS, Millar J, Wetzel SG, Wanke I, Rüfenacht DA. Flow diversion treatment: intra-aneurismal blood flow velocity and WSS reduction are parameters to predict aneurysm thrombosis. *Acta Neurochir (Wien)* 2012, 154:1827-1834.
163. Ouared R, Larrabide I, Brina O, Bouillot P, Erceg G, Yilmaz H, Lovblad K-O, Pereira VM. Computational fluid dynamics analysis of flow reduction induced by flow-diverting stents in intracranial aneurysms: a patient-unspecific hemodynamics change perspective. *J Neurointerv Surg* 2016, 8:1288-1293.

164. Tan KT, Lip GY. Red vs white thrombi: treating the right clot is crucial. *Arch Intern Med* 2003, 163:2534-2535.
165. Levitt MR, Barbour MC, du Roscoat SR, Geindreau C, Chivukula VK, McGah PM, Nerva JD, Morton RP, Kim LJ, Aliseda A. Computational fluid dynamics of cerebral aneurysm coiling using high-resolution and high-energy synchrotron X-ray microtomography: comparison with the homogeneous porous medium approach. *J Neurointerv Surg* 2016:Published Online First: 12 July 2016, doi: 2010.1136/neurintsurg-2016-012479.
166. Raschi M, Mut F, Löhner R, Cebral J. Strategy for modeling flow diverters in cerebral aneurysms as a porous medium. *Int J Numer Method Biomed Eng* 2014, 30:909-925.
167. Bouillot P, Brina O, Yilmaz H, Farhat M, Erceg G, Lovblad K-O, Vargas M, Kulcsar Z, Pereira V. Virtual-versus-Real Implantation of Flow Diverters: Clinical Potential and Influence of Vascular Geometry. *Am J Neuroradiol* 2016, 37:2079-2086.
168. Gao B, Baharoglu M, Cohen A, Malek A. Stent-assisted coiling of intracranial bifurcation aneurysms leads to immediate and delayed intracranial vascular angle remodeling. *Am J Neuroradiol* 2012, 33:649-654.
169. King R, Chueh J-Y, van der Bom I, Silva C, Carniato S, Spilberg G, Wakhloo A, Gounis M. The effect of intracranial stent implantation on the curvature of the cerebrovasculature. *Am J Neuroradiol* 2012, 33:1657-1662.
170. Kono K, Shintani A, Terada T. Hemodynamic effects of stent struts versus straightening of vessels in stent-assisted coil embolization for sidewall cerebral aneurysms. *PLoS One* 2014, 9:e108033.
171. Fiorella D, Woo HH, Albuquerque FC, Nelson PK. Definitive reconstruction of circumferential, fusiform intracranial aneurysms with the Pipeline embolization device. *Neurosurgery* 2008, 62:1115-1121.
172. Mut F, Ruijters D, Babic D, Bleise C, Lylyk P, Cebral JR. Effects of changing physiologic conditions on the in vivo quantification of hemodynamic variables in cerebral aneurysms treated with flow diverting devices. *Int J Numer Method Biomed Eng* 2014, 30:135-142.
173. Whittle I, Dorsch NW, Besser M. Spontaneous thrombosis in giant intracranial aneurysms. *J Neurol Neurosurg Psychiatry* 1982, 45:1040-1047.
174. Brinjikji W, Kallmes DF, Kadirvel R. Mechanisms of healing in coiled intracranial aneurysms: a review of the literature. *Am J Neuroradiol* 2015, 36:1216-1222.
175. Szikora I, Berentei Z, Kulcsar Z, Marosfoi M, Vajda Z, Lee W, Berez A, Nelson PK. Treatment of intracranial aneurysms by functional reconstruction of the parent artery: the Budapest experience with the Pipeline embolization device. *Am J Neuroradiol* 2010, 31:1139-1147.
176. Lylyk P, Miranda C, Ceratto R, Ferrario A, Scrivano E, Luna HR, Berez AL, Tran Q, Nelson PK, Fiorella D. Curative endovascular reconstruction of cerebral aneurysms with the Pipeline embolization device: the Buenos Aires experience. *Neurosurgery* 2009, 64:632-643.
177. Crobeddu E, Lanzino G, Kallmes DF, Cloft H. Review of 2 decades of aneurysm-recurrence literature, part 1: reducing recurrence after endovascular coiling. *Am J Neuroradiol* 2013, 34:266-270.
178. Crobeddu E, Lanzino G, Kallmes DF, Cloft H. Review of 2 decades of aneurysm-recurrence literature, part 2: managing recurrence after endovascular coiling. *Am J Neuroradiol* 2013, 34:481-485.
179. Siddiqui AH, Abla AA, Kan P, Dumont TM, Jahshan S, Britz GW, Hopkins LN, Levy EI. Panacea or problem: flow diverters in the treatment of symptomatic large or giant fusiform vertebrobasilar aneurysms: Clinical article. *J Neurosurg* 2012, 116:1258-1266.
180. Fischer S, Vajda Z, Perez MA, Schmid E, Hopf N, Bäzner H, Henkes H. Pipeline embolization device (PED) for neurovascular reconstruction: initial experience in the treatment of 101 intracranial aneurysms and dissections. *Neuroradiology* 2012, 54:369-382.

181. Frösen J, Tulamo R, Paetau A, Laaksamo E, Korja M, Laakso A, Niemelä M, Hernesniemi J. Saccular intracranial aneurysm: pathology and mechanisms. *Acta Neuropathol* 2012, 123:773-786.
182. Hoffman M. A cell-based model of coagulation and the role of factor VIIa. *Blood Rev* 2003, 17:S1-S5.
183. Himburg HA, Dowd SE, Friedman MH. Frequency-dependent response of the vascular endothelium to pulsatile shear stress. *Am J Physiol-Heart C* 2007, 293:H645-H653.
184. Li Y-D, Ye B-Q, Zheng S-X, Wang J-T, Wang J-G, Chen M, Liu J-G, Pei X-H, Wang L-J, Lin Z-X. NF-κB transcription factor p50 critically regulates tissue factor in deep vein thrombosis. *J Biol Chem* 2009, 284:4473-4483.
185. Mackman N. Role of tissue factor in hemostasis, thrombosis, and vascular development. *Arterioscler Thromb Vasc Biol* 2004, 24:1015-1022.
186. Biasetti J, Gasser TC, Auer M, Hedin U, Labruto F. Hemodynamics of the normal aorta compared to fusiform and saccular abdominal aortic aneurysms with emphasis on a potential thrombus formation mechanism. *Ann Biomed Eng* 2010, 38:380-390.
187. Biasetti J, Hussain F, Gasser TC. Blood flow and coherent vortices in the normal and aneurysmatic aortas: a fluid dynamical approach to intra-luminal thrombus formation. *J Roy Soc Interface* 2011, 8:1449–1461.
188. Davies PF. Flow-mediated endothelial mechanotransduction. *Physiol Rev* 1995, 75:519-560.
189. Bodnár T, Fasano A, Sequeira A. Mathematical models for blood coagulation. In: *Fluid-Structure Interaction and Biomedical Applications*: Springer; 2014, 483-569.
190. Chatterjee MS, Denney WS, Jing H, Diamond SL. Systems biology of coagulation initiation: kinetics of thrombin generation in resting and activated human blood. *PLoS Comput Biol* 2010, 6:e1000950.
191. Chong W, Zhang Y, Qian Y, Lai L, Parker G, Mitchell K. Computational hemodynamics analysis of intracranial aneurysms treated with flow diverters: correlation with clinical outcomes. *Am J Neuroradiol* 2014, 35:136-142.
192. Malaspinas O, Turjman A, de Sousa DR, Garcia-Cardena G, Raes M, Nguyen P-T, Zhang Y, Courbebaisse G, Lelubre C, Boudjeltia KZ. A spatio-temporal model for spontaneous thrombus formation in cerebral aneurysms. *J Theor Biol* 2016.
193. Ou C, Huang W, Yuen MM-F. A computational model based on fibrin accumulation for the prediction of stasis thrombosis following flow-diverting treatment in cerebral aneurysms. *Med Biol Eng Comput* 2016:1-11.
194. Koskinas KC, Chatzizisis YS, Antoniadis AP, Giannoglou GD. Role of endothelial shear stress in stent restenosis and thrombosis: pathophysiologic mechanisms and implications for clinical translation. *J Am Coll Cardiol* 2012, 59:1337-1349.
195. Rayz V, Boussel L, Ge L, Leach J, Martin A, Lawton M, McCulloch C, Saloner D. Flow residence time and regions of intraluminal thrombus deposition in intracranial aneurysms. *Ann Biomed Eng* 2010, 38:3058-3069.
196. Ouared R, Chopard B. Lattice Boltzmann simulations of blood flow: non-Newtonian rheology and clotting processes. *J Stat Phys* 2005, 121:209-221.
197. Zimny S, Chopard B, Malaspinas O, Lorenz E, Jain K, Roller S, Bernsdorf J. A multiscale approach for the coupled simulation of blood flow and thrombus formation in intracranial aneurysms. *Procedia Comput Sc* 2013, 18:1006-1015.
198. Biasetti J, Spazzini PG, Swedenborg J, Gasser TC. An integrated fluid-chemical model toward modeling the formation of intra-luminal thrombus in abdominal aortic aneurysms. *Front Physiol* 2012, 3:266.
199. Ngoepe MN, Ventikos Y. Computational modelling of clot development in patient-specific cerebral aneurysm cases. *J Thromb Haemost* 2015, 14:262-272.

200. Cito S, Mazzeo MD, Badimon L. A review of macroscopic thrombus modeling methods. *Thromb Res* 2013, 131:116-124.
201. Danforth CM, Orfeo T, Mann KG, Brummel-Ziedins KE, Everse SJ. The impact of uncertainty in a blood coagulation model. *Math Med Biol* 2009, 26:323-336.
202. Luan D, Szlam F, Tanaka KA, Barie PS, Varner JD. Ensembles of uncertain mathematical models can identify network response to therapeutic interventions. *Mol Biosyst* 2010, 6:2272-2286.
203. Luan D, Zai M, Varner JD. Computationally derived points of fragility of a human cascade are consistent with current therapeutic strategies. *PLoS Comput Biol* 2007, 3:e142.
204. Moiseyev G, Bar-Yoseph PZ. Computational modeling of thrombosis as a tool in the design and optimization of vascular implants. *J Biomech* 2013, 46:248-252.
205. Ogilvy CS, Chua MH, Fusco MR, Griessenauer CJ, Harrigan MR, Sonig A, Siddiqui AH, Levy EI, Snyder K, Avery M. Validation of a system to predict recanalization after endovascular treatment of intracranial aneurysms. *Neurosurgery* 2015, 77:168-174.
206. Ogilvy CS, Chua MH, Fusco MR, Reddy AS, Thomas AJ. Stratification of recanalization for patients with endovascular treatment of intracranial aneurysms. *Neurosurgery* 2015, 76:390-395.
207. Arzani A, Gambaruto AM, Chen G, Shadden SC. Lagrangian wall shear stress structures and near-wall transport in high-Schmidt-number aneurysmal flows. *J Fluid Mech* 2016, 790:158-172.
208. Cebral JR, Meng H. Counterpoint: realizing the clinical utility of computational fluid dynamics—closing the gap. *Am J Neuroradiol* 2012, 33:396-398.
209. Hennig P, Osborne MA, Girolami M. Probabilistic numerics and uncertainty in computations. In: *P R Soc A*; 2015, 20150142.
210. Sankaran S, Grady L, Taylor CA. Impact of geometric uncertainty on hemodynamic simulations using machine learning. *Comput Method Appl M* 2015, 297:167-190.
211. Schneiders J, Marquering H, Antiga L, Van den Berg R, VanBavel E, Majoie C. Intracranial aneurysm neck size overestimation with 3D rotational angiography: the impact on intra-aneurysmal hemodynamics simulated with computational fluid dynamics. *Am J Neuroradiol* 2013, 34:121-128.

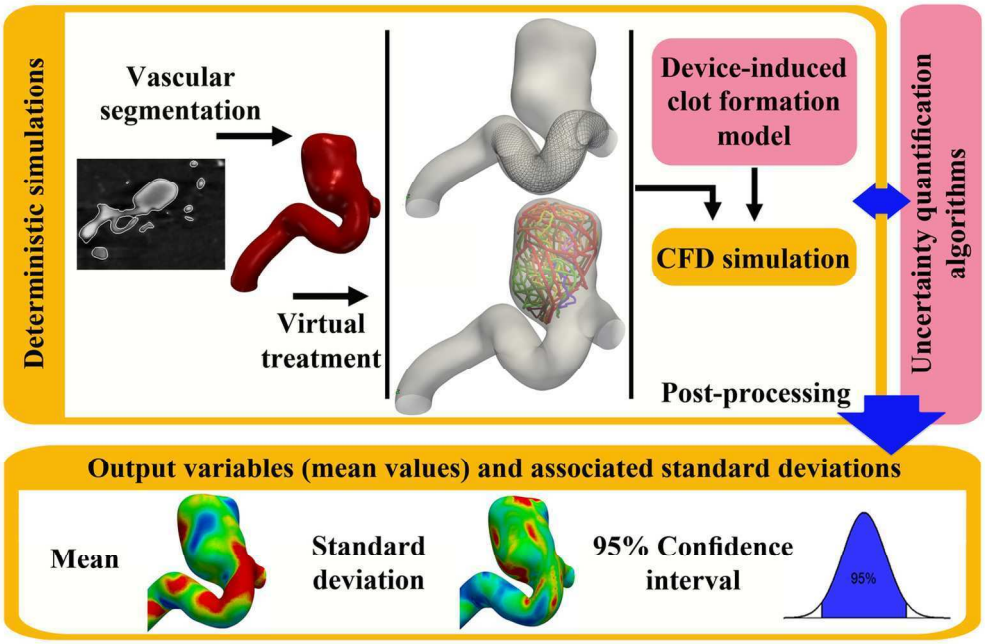

64x41mm (600 x 600 DPI)

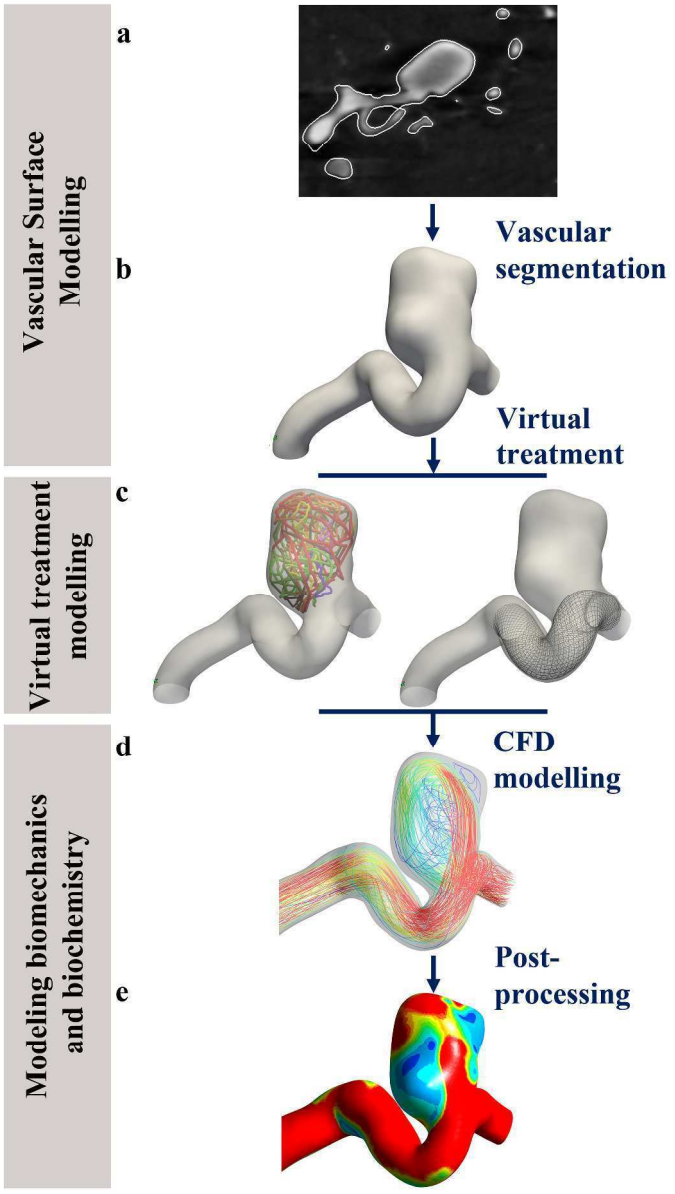

Figure 1. An ideal virtual endovascular treatment model is comprised of sub-models in which the vascular surface, virtual treatment, and biomechanics and biochemistry are modelled, respectively. Patient's angiogram (a) is segmented and a vascular surface model (b) is reconstructed and used for virtual treatment with coils or flow diverting stents (c). CFD simulations then are performed to calculate blood velocity field (d) in the presence of device-induced intra-aneurysmal clot, from which the shear stresses on the vessel wall (e) can be computed.

Figure 1
111x194mm (600 x 600 DPI)

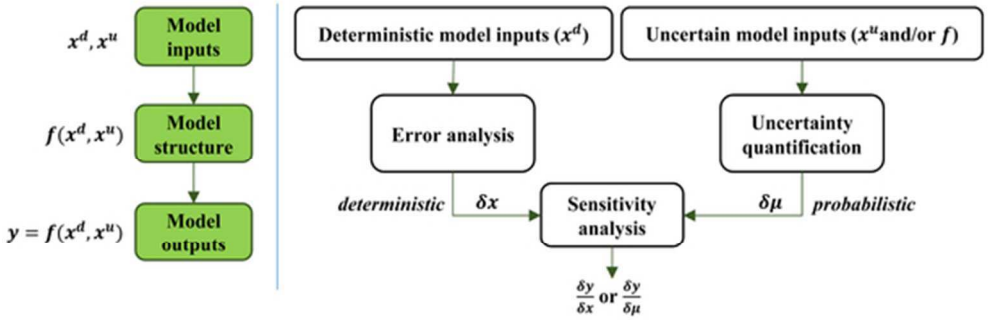

Figure 2. The left panel shows overall structure of a typical mathematical model with x^d and x^u as vectors of deterministic and uncertain model inputs, respectively; f describing the model structure; and y as vector of model outputs. The right panel shows error analysis and uncertainty quantification as processes to identify and quantify errors and uncertainties, respectively; and sensitivity analysis as a process to propagate the quantified errors and uncertainties to the model outputs.
Figure 2
52x17mm (300 x 300 DPI)

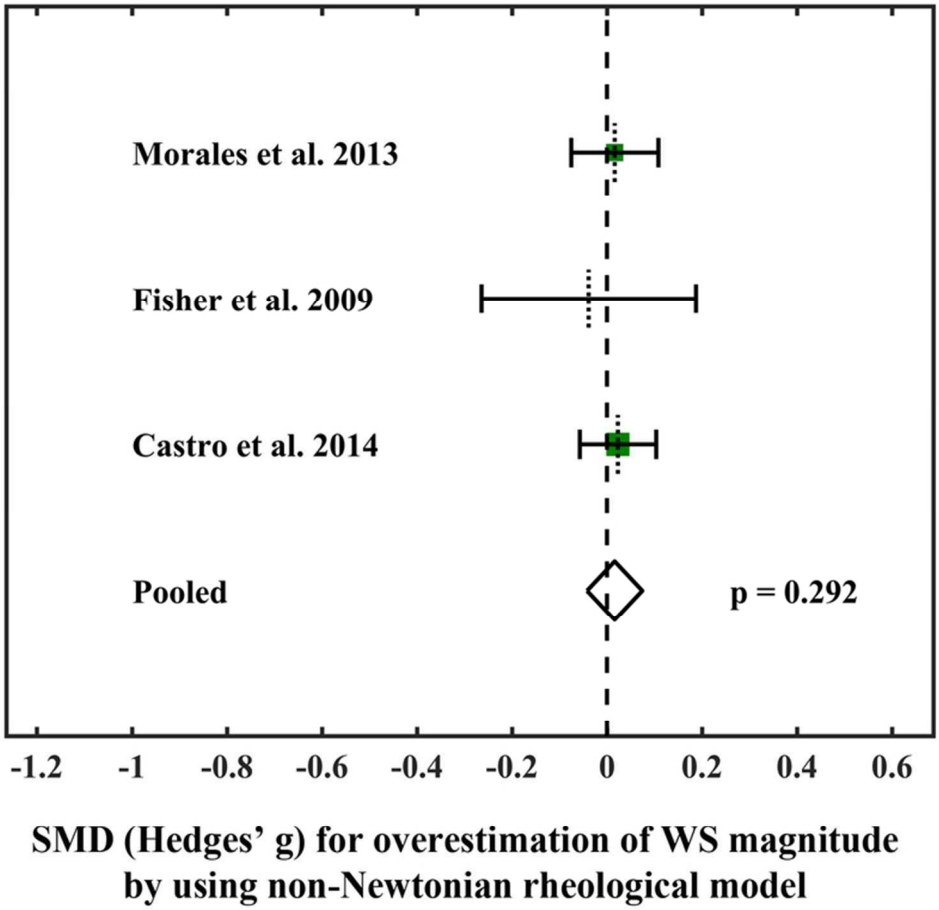

Figure 3. Forest plot showing the overestimation of space-and-time-averaged aneurysmal WSS produced by the non-Newtonian blood rheology. The plot illustrates effect sizes, Hedges' g, (represented by a square) and the confidence intervals (the horizontal lines) for each study and the pooled effect (the centre of the diamond) and its confidence interval (the width of the diamond) across all studies. Vertical dotted lines for each study show the study mean and the green squares are sized according to the study weight.
Figure 3
70x66mm (300 x 300 DPI)

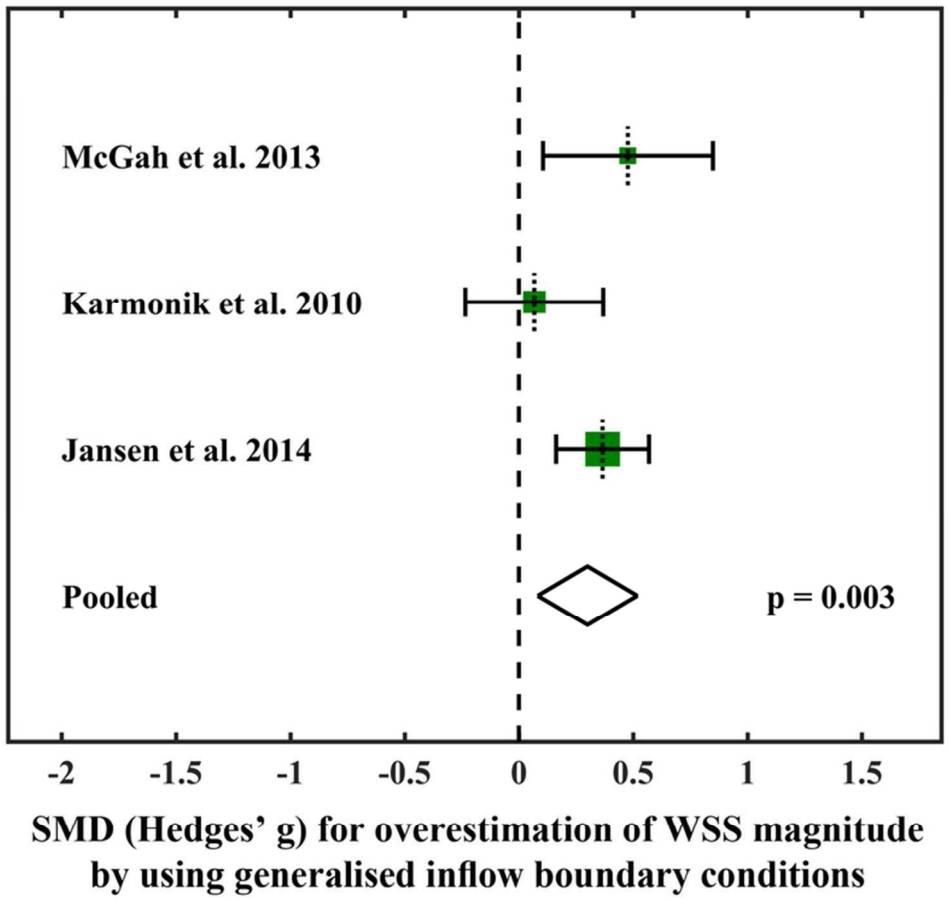

Figure 4. Forest plot showing the overestimation of space-and-time-averaged aneurysmal WSS produced by the generalised inflow boundary conditions. The plot illustrates effect sizes, Hedges' g, (represented by a square) and the confidence intervals (the horizontal lines) for each study and the pooled effect (the centre of the diamond) and its confidence interval (the width of the diamond) across all studies. Vertical dotted lines for each study show the study mean and the green squares are sized according to the study weight.
Figure 4
70x65mm (300 x 300 DPI)

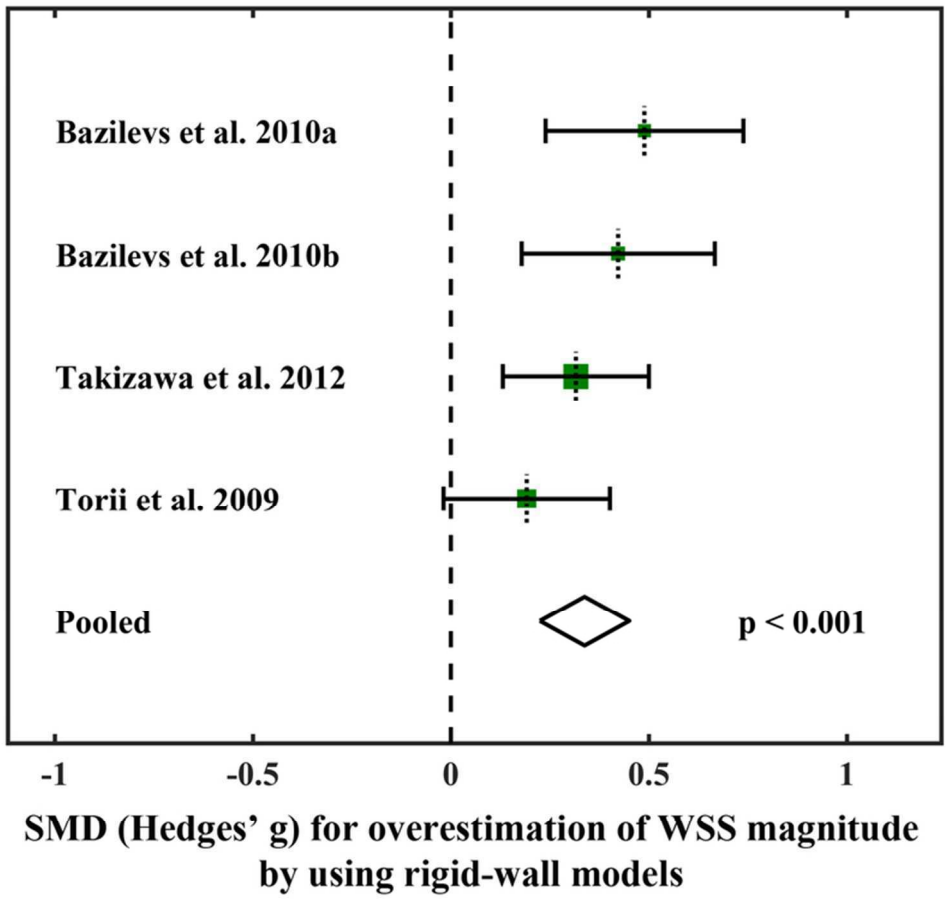

Figure 5. Forest plot showing the overestimation of maximum peak systolic aneurysmal WSS produced by the rigid arterial wall assumption. The plot illustrates effect sizes, Hedges' g, (represented by a square) and the confidence intervals (the horizontal lines) for each study and the pooled effect (the centre of the diamond) and its confidence interval (the width of the diamond) across all studies. Vertical dotted lines for each study show the study mean and the green squares are sized according to the study weight.
Figure 5
70x66mm (300 x 300 DPI)

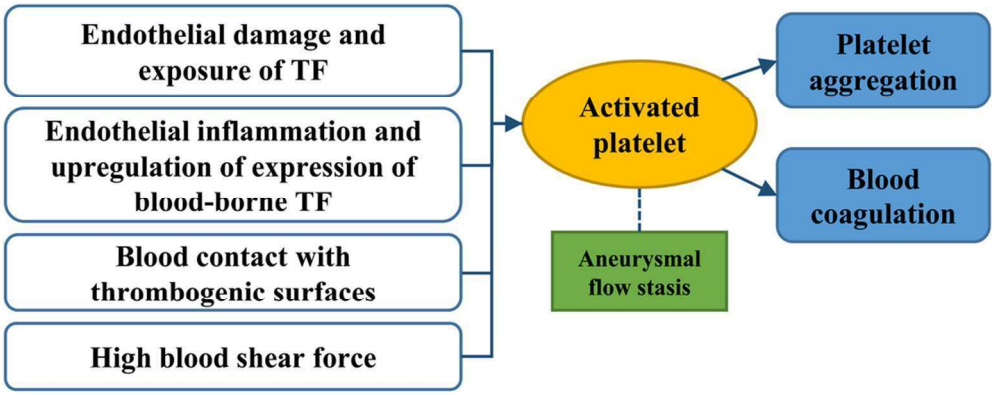

Figure 6. Possible mechanisms of intra-aneurysmal thrombosis
Figure 6
48x19mm (600 x 600 DPI)